Neurobiology of Disease 187 (2023) 106300

Contents lists available at ScienceDirect

Neurobiology of Disease

journal homepage: www.elsevier.com/locate/ynbdi

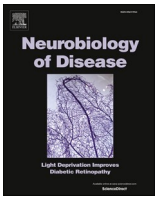

A murine model of *BSCL2*-associated Celia's encephalopathy

Silvia Cobelo-Gómez [a,1], Sofía Sánchez-Iglesias [a,1], Alberto Rábano [b], Ana Senra [c], Pablo Aguiar [d,e], Noemí Gómez-Lado [d,e], Lara García-Varela [d,e], Iván Burgueño-García [b], Laura Lampón-Fernández [a], Antía Fernández-Pombo [a,f], Everardo Josué Díaz-López [a,f], Teresa Prado-Moraña [a,f], Beatriz San Millán [g,h], David Araújo-Vilar [a,f,*]

[a] *UETeM-Molecular Pathology Group. Department of Psychiatry, Radiology, Public Health, Nursing and Medicine, IDIS-CIMUS, University of Santiago de Compostela, Spain*
[b] *Alzheimer's Disease Research Unit, CIEN Foundation, Queen Sofia Foundation Alzheimer Center, Madrid, Spain*
[c] *Department of Physiology, CIMUS, University of Santiago de Compostela, Spain*
[d] *Molecular Imaging and Medical Physics, University of Santiago de Compostela-IDIS, Spain*
[e] *Nuclear Medicine and Molecular Imaging Group, IDIS, University Clinical Hospital of Santiago de Compostela, Spain*
[f] *Division of Endocrinology and Nutrition, University Clinical Hospital of Santiago de Compostela, Spain*
[g] *Grupo de Enfermedades Raras y Medicina Pediátrica, Instituto de Investigación Sanitaria Galicia Sur (IISGS), Vigo, Spain*
[h] *Pathology Department, Alvaro Cunqueiro Hospital, Vigo, Spain*

ARTICLE INFO

Keywords:
BSCL2
Seipin
PELD
Transgenic mouse
Neurodegeneration
Celia's encephalopathy

ABSTRACT

Celia's encephalopathy or progressive encephalopathy with/without lipodystrophy is a neurodegenerative disease with a fatal prognosis in childhood. It is generally caused by the c.985C > T variant in the *BSCL2* gene, leading to the skipping of exon 7 and resulting in an aberrant seipin protein (Celia-seipin).

To precisely define the temporal evolution and the mechanisms involved in neurodegeneration, lipodystrophy and fatty liver in Celia's encephalopathy, our group has generated the first global knock-in murine model for the aberrant human transcript of *BSCL2* (*Bscl2*$^{Celia/Celia}$) using a strategy based on the Cre/loxP recombination system. In order to carry out a characterization at the neurological, adipose tissue and hepatic level, behavioral studies, brain PET, metabolic, histological and molecular studies were performed.

Around 12% of homozygous and 5.4% of heterozygous knock-in mice showed severe neurological symptoms early in life, and their life expectancy was dramatically reduced. Severe generalized lipodystrophy and mild hepatic steatosis were present in these affected animals, while serum triglycerides and glucose metabolism were normal, with no insulin resistance. Furthermore, the study revealed a reduction in brain glucose uptake, along with patchy loss of Purkinje cells and the presence of intranuclear inclusions in cerebellar cortex cells. Homozygous, non-severely-affected knock-in mice showed a decrease in locomotor activity and greater anxiety compared with their wild type littermates.

Bscl2$^{Celia/Celia}$ is the first murine model of Celia's encephalopathy which partially recapitulates the phenotype and severe neurodegenerative picture suffered by these patients. This model will provide a helpful tool to

Abbreviations: AUC, area under the curve; BAC, bacterial artificial chromosome; BAT, brown adipose tissue; BC, citrate buffer; *BSCL2* and *Bscl2*, Berardinelli-Seip congenital lipodystrophy 2; *Cat*, catalase; CD68, cluster of differentiation 68; CT, computed tomography; DTA, diphtheria toxin A; ESC, embryonic stem cells; GAPDH, Glyceraldehyde-3-Phosphate Dehydrogenase; GFAP, glial fibrillary acidic protein; *Gng3*, Guanine nucleotide-binding protein G subunit gamma-3; gonWAT, gonadal white adipose tissue; *Gpx1*, glutathione peroxidase 1; GTT, glucose tolerance test; H&E, hematoxylin and eosin; HAs, homology arms region; iBAT, interscapular brown adipose tissue; ingWAT, inguinal white adipose tissue; ITT, insulin tolerance test; LD, lipid droplet; MLEM, maximum likelihood expectation maximization; PELD, progressive encephalopathy with/without lipodystrophy; *Pex11g*, peroxisomal biogenesis factor 11 gamma; *Pex16*, peroxisomal biogenesis factor 16; *Pparg*, peroxisome proliferator activated receptor gamma; qPCR, quantitative polymerase chain reaction; *Rn18s*, 18S ribosomal RNA; RT, room temperature; RTU, ready-to-use; S.A., severely affected; SKO, seipin knock-out mice; *Sod1*, superoxide dismutase 1; *Sod2*, superoxide dismutase 2; SUV_{mean}, mean standardized uptake value; TBS, Tris-buffered saline; TE, Tris-EDTA; TG, transgene; VOIs, volume of interest; WAT, white adipose tissue..

* Corresponding author at: U.E.T.eM., CIMUS-Faculty of Medicine, University of Santiago de Compostela, Avda de Barcelona s/n, 15707 Santiago de Compostela, Spain.
E-mail address: david.araujo@usc.es (D. Araújo-Vilar).
[1] These authors contributed equally to this manuscript.

https://doi.org/10.1016/j.nbd.2023.106300
Received 3 June 2023; Received in revised form 6 September 2023; Accepted 14 September 2023
Available online 16 September 2023

investigate both the progressive encephalopathy with/without lipodystrophy and congenital generalized lipodystrophy.

1. Introduction

Celia's encephalopathy, or progressive encephalopathy with/without lipodystrophy (PELD) (MIM: #615924), is a pediatric neurodegenerative disease with a fatal prognosis, which was first described by our group in 2013 (Guillen-Navarro et al., 2013; Ruiz-Riquelme et al., 2015a). Celia's encephalopathy begins to manifest from the age of 2 via psychomotor retardation with significant language impairment. Neurological regression begins at 3–4 years of age, with a sudden onset (4 years) of severe myoclonic epilepsy, spastic tetraparesis, and severe encephalopathy, leading to death before the age of 9 years (average 7 years) (Guillen-Navarro et al., 2013; Sánchez-Iglesias et al., 2021; Araujo-Vilar and Santini, 2019).

This extremely rare disease (with only 23 cases have been reported to date (Sánchez-Iglesias et al., 2021)) is generally a consequence of the c.985C > T variant (rs587777606) in the *BSCL2* gene in homozygosis or in compound heterozygosis (when the patient carries a PELD variant in one allele and other variant in the other -in *trans*- of the *BSCL2* gene). The *BSCL2* gene encodes for seipin (NM_001122955.3), a resident protein of the endoplasmic reticulum with two transmembrane domains, an intraluminal loop and two amino and carboxy-terminal tails in the cytoplasm. In humans, seipin forms 11–12-units homoligomers that make up a toroid (Sim et al., 2013; Yan et al., 2018; Sim et al., 2020). The main function of seipin, an evolutionarily highly conserved protein, is to modulate lipid droplet (LD) formation (Rao and Goodman, 2021). Three seipin isoforms are mainly encode by this gene, of 462 (*BSCL2*–203 ENST00000360796.9; CCDS44627), 398 (*BSCL2*–205/207/210, ENST00000403550.5; ENST00000407022.7; ENST00000421906.5; CCDS8031), and 287 (*BSCL2*–201, ENST00000278893.11; CCDS55769) amino acids long, respectively (Cartwright and Goodman, 2012). In humans, this gene has its greatest expression, not in adipose tissue as is to be expected, but in the central nervous system, pituitary gland and testes (Guillen-Navarro et al., 2013; Magre et al., 2001). *BSCL2*–203 is primarily expressed in the brain (78.9%), whereas in other tissues the expression of *BSCL2*–203 and *BSCL2*–205/207/210 transcripts is similar, and *BSCL2*–201 expression is negligible in all tissues (< 1%) (Sanchez-Iglesias et al., 2019a).

In PELD, the c.985C > T variant impairs the splicing process leading to the skipping of the whole exon 7. Consequently, the gene will encode for an aberrant seipin (Celia-seipin), with a different amino acid sequence to the wild type isoform *BSCL2*–203 downstream of exon 6, losing the second transmembrane domain (Guillen-Navarro et al., 2013). This aberrant seipin forms macroaggregates, causing endoplasmic reticulum stress, activating the unfolded protein response and driving neurons to apoptosis (Ruiz-Riquelme et al., 2015b).

Knowledge of the pathogenic mechanisms of Celia's Encephalopathy, of which a part has been elucidated above, implies the development of biological models of the disease, since its low prevalence, severity and mainly affected organ (the brain) make it difficult to study in humans. Therefore, our group has generated the first murine model for this disease. Specifically, it is a global knock-in mouse that expresses the aberrant human transcript of *BSCL2* in all tissues and that has made it possible to clarify the temporal evolution of the disease from the postnatal period to the end of life of these animals. Furthermore, it has enabled studies to be carried out to gain an in-depth knowledge of the molecular mechanisms involved in neurodegeneration, lipodystrophy and fatty liver, among other comorbidities associated to seipinopathies.

2. Methods

2.1. Animals

2.1.1. Generation of *Bscl2*$^{Celia/Celia}$ mice

The *Bscl2* gene (GenBank accession number: NM_001290823.1, Ensembl: ENSMUSG00000071657) is located on mouse chromosome 19. Eleven exons have been identified, with a second ATG start codon in exon 2 (Transcript: Bscl2–008 ENSMUST00000086058) (Fig. 1a). For the knock-in model (*Bscl2*$^{Celia/Celia}$), the ATG start codon in exon 2 of the *Bscl2* gene was replaced with a reversely positioned cassette (LoxP-Lox2272-reverse His tag-Human *BSCL2* CDS without exon7-reverse LoxP-Neo cassette-reverse Lox2272) (Fig. 1b-c) in such a way that in the targeted allele the human transgene (3′-5′) was not transcribed before Cre mediated recombination. In the presence of Cre recombinase, the inversion of the cassette led to the expression of His-tagged, aberrant human seipin (Fig. 1e). To engineer the targeting vector, homology arms region (HAs) was generated by PCR using bacterial artificial chromosome (BAC) clone RP23-83P21 and RP23-125I21 from the C57BL/6 J library as template. In the targeting vector, the Neo cassette was flanked by Frt sites (Fig. 1b-c). Diphtheria toxin A (DTA) was used for negative selection. C57BL/6 embryonic stem cells (ESC) were used for gene targeting.

Mouse genomic fragments containing HAs were amplified from BAC clone using high fidelity Taq and were sequentially assembled into a targeting vector, together with recombination sites and selection markers, as shown in Fig. 1b. The targeting vector was digested by restriction enzymes for confirmation purposes. The linearized vector was subsequently delivered into ESC (C57BL/6) via electroporation, followed by drug selection, PCR screening, and Southern blot confirmation. After confirming correctly targeted ESC clones via Southern blotting, some clones were selected for blastocyst microinjection, followed by chimera production. Founders F0 were confirmed as germline-transmitted via crossbreeding with an Flp-deleter mouse. One of the founders, a male heterozygous seipin knock-out mouse (*Bscl2*$^{+/-}$), was bred with a Cre-global female mouse (E2a-Cre, 2.B6.FVB-Tg(EIIa-cre) C5379Lmgd/J, ref. J003724, The Jackson Laboratory, http://jaxmice.jax.org/strain/003724.html) to obtain the heterozygous constitutive KI mice (*Bscl2*$^{+/Celia}$). This required a round of intercrossing to obtain homozygous mice (*Bscl2*$^{Celia/Celia}$) (Fig. 2). The transgene sequence was confirmed by sequencing. This model was developed in collaboration with Cyagen (Santa Clara, US).

2.1.2. Maintenance and care of animals

The animals were housed in ventilated racks and cages under specific pathogen-free conditions. Room temperature (22 °C ± 1 °C), humidity (55% ± 2%) and light/dark rhythm (12:12) were all controlled. All mice had ad libitum access to water and standard feed (Teklad Global 18% Protein Rodent Diet, Envigo). Phenotypic, weight and behavior monitoring were carried out throughout the whole life of the animals.

2.1.3. Genotyping protocol

Isolation of genomic DNA was carried out using E.Z.N.A Tissue DNA Kit (Omega Bio-tek, Norcross, United States). Seven specific primers were designed with the Primer3Plus software (http://www.bioinformatics.nl/cgi-bin/primer3plus/primer3plus.cgi) and used as four different combinations. PCR conditions and primers are available upon request. Samples were analyzed on a 1% agarose gel.

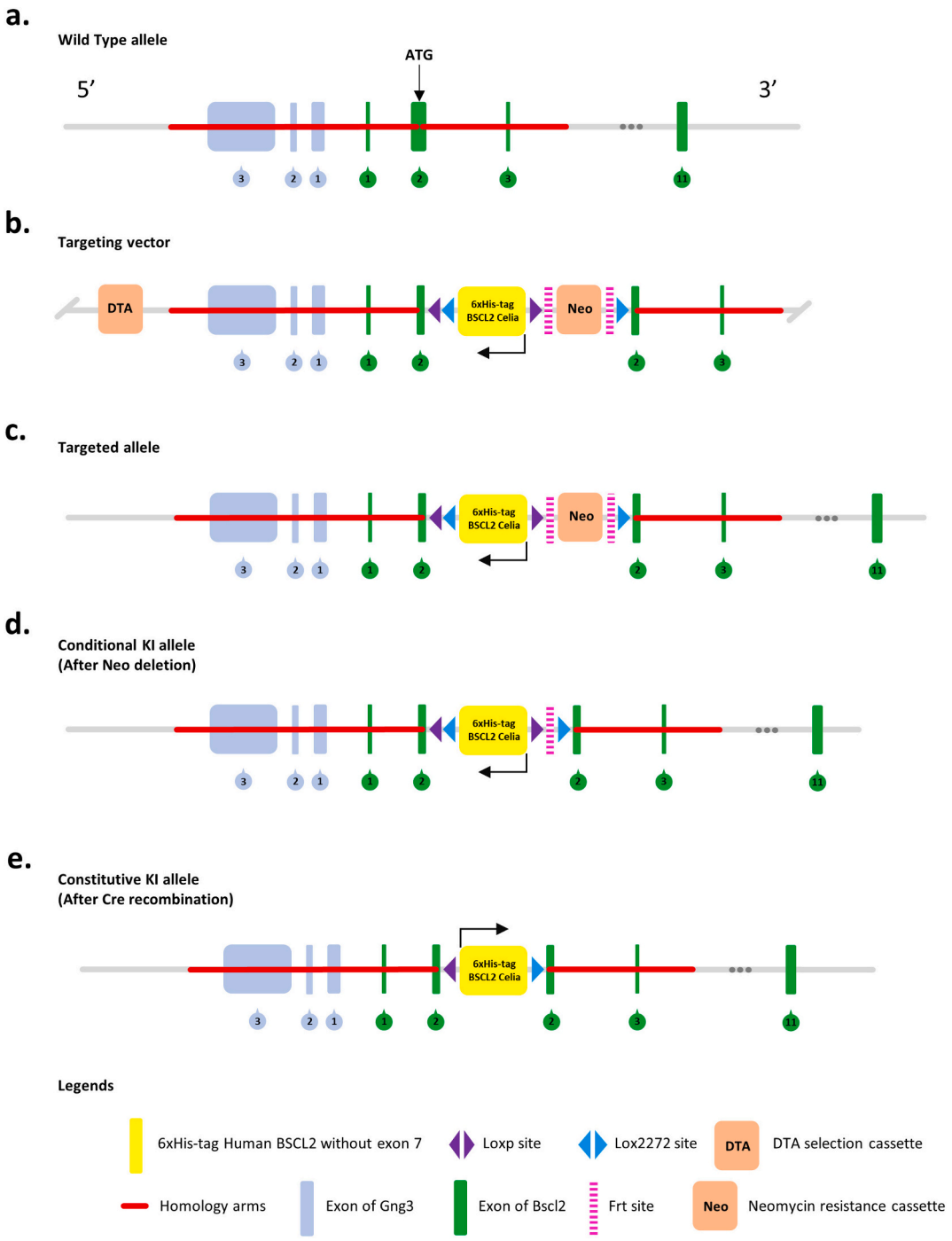

Fig. 1. Targeting strategy for the *BSCL2* knock-in (KI) murine model. a. Wild type allele (Transcript: Bscl2–008). b. Targeting vector. c. Targeting allele. d. Conditional knock-in allele after Neo deletion. e. Constitutive knock-in allele after Cre recombination.

2.2. Behavioral tests

On the day of testing, the mice were weighed and kept in their home cages, allowing them to acclimatize to the red-light-controlled testing room (4 lx) for at least 60 min. The testing sequence was such that tests involving lower stress levels preceded those involving higher stress levels, as follows: open field test, elevated zero maze, rotarod test, beam walking test, wire hang test and Morris water maze. The tests were spaced by at least 2 weeks. The behavioral experiments that required video capture were recorded by an overhead camera linked to a computer with AnyMaze Video Tracking software (v. 7.16, Stoelting) to track the position of the animals.

2.2.1. NeuroScore and welfare state

Mice were scored from 0 (normal) to 4 (severely impaired) for all the tests. For NeuroScore assessment, the following tests were considered: hindlimb and forelimb flexion tests to check hindlimb and forelimb functions; lateral pulsion task test to verify the coordination of all four limbs and vibrissae-evoked forelimb placing test to assess asymmetry in the sensorimotor cortex and striatum (Encarnacion et al., 2011; Febinger et al., 2016; Schaar et al., 2010). Furthermore, the welfare state of the mice was evaluated taking into account the following characteristics: tremor, kyphosis, fur and motion.

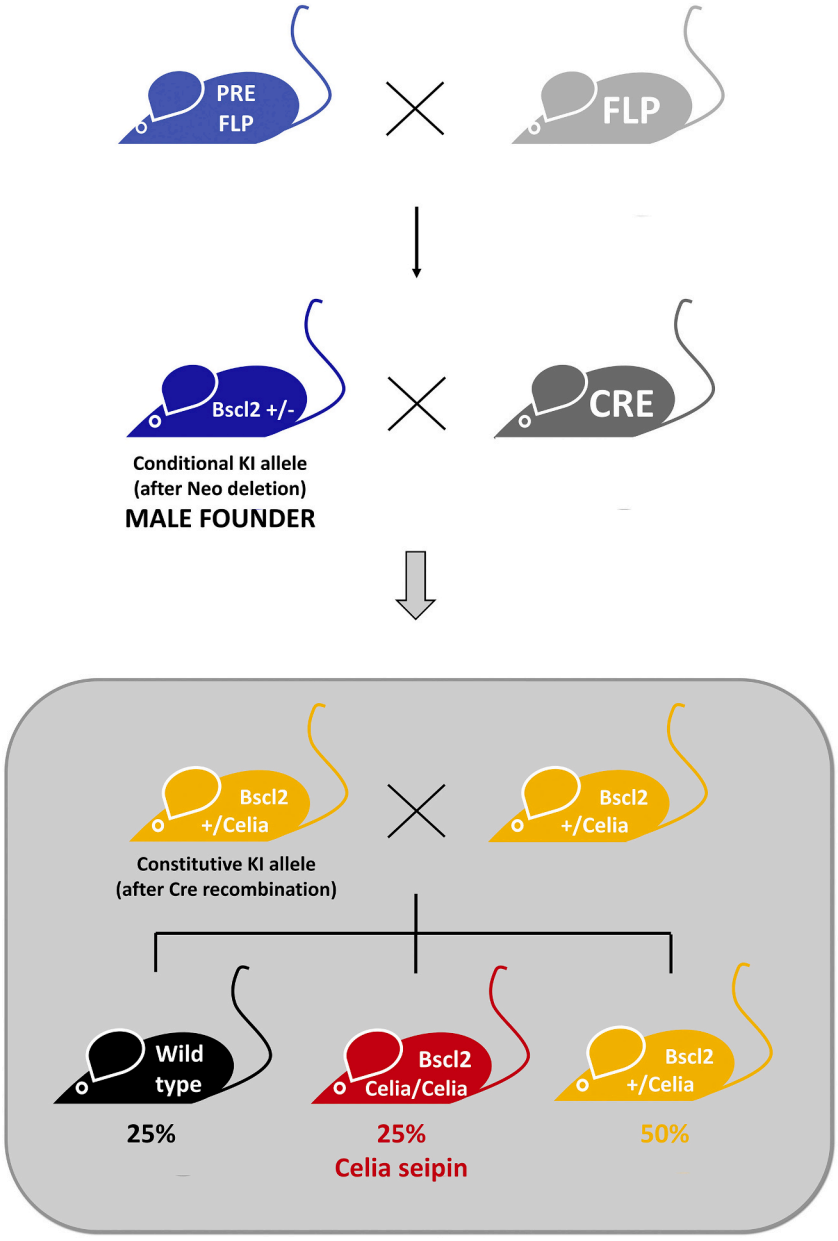

Fig. 2. Germline transmission for the *BSCL2* knock-in (KI) murine model generation. A mouse with the targeting allele (PRE FLP) was crossbred with an Flp-deleter mouse (FLP) in order to obtain a male founder, a mouse with the conditional KI allele. This heterozygous knock-out mouse (*Bscl2*$^{+/-}$) was then crossbred with a Cre-global female for the generation of mice with the constitutive KI allele (*Bscl2*$^{+/Celia}$). Subsequent intercrossing was needed to generate 25% wild type, 25% homozygous (*Bscl2*$^{Celia/Celia}$) and 50% heterozygous (*Bscl2*$^{+/Celia}$) mice.

2.2.2. Open field test

The mice were examined in a cuboid plexiglass box (45 cm × 45 cm × 40 cm) with the floor divided into 9 equal squares. The central zone was defined as the central square (15 cm × 15 cm). Each mouse was placed in the center zone of the arena and allowed to explore freely for 6 min. The mice were test daily for a total of four consecutive days (1 habituation trial and 3 replicates) (Tatem et al., 2014; Seibenhener and Wooten, 2015). The following parameters were evaluated: total distance travelled, mean speed, moving time, time spent in the center region of the area, number of times each mouse crossed the area from top to bottom and from left to right.

2.2.3. Elevated zero maze

The elevated zero maze is raised to a height of 64 cm above the floor and consists of four equal quadrants; two opposite quadrants are darkened and enclosed, with the remaining two being open and exposed. The maze is 70 cm in diameter and runway width is 5 cm. The mice were tested daily for a total of four consecutive days (1 habituation trial and 3 replicates). To start the test, the animal was placed at a randomly chosen boundary between an open and a closed zone, facing the inside of the closed zone. The tests were 5 min in duration (Shepherd et al., 1994; O'Leary et al., 2013). The following parameters were analyzed: total distance travelled, mean speed, moving time, still time, rotations, time spent in the open and/or closed zones of the mazes.

2.2.4. Rotarod test

The RotaRod apparatus (Ugo Basile, Gemonio, Italy) was used to perform the experiment. All mice were trained for four consecutive days and given three trials per day, separated by 30-min inter-trial intervals. The rotarod was set at a starting speed of 5 rpm with continuous acceleration for 90 s, up to a speed of 44 rpm (Deacon, 2013a; Brooks and Dunnett, 2009). The mean distance was recorded. In the case of a full passive rotation, the timer was stopped, and the previous data also recorded.

2.2.5. Beam walking test

The goal of this test is for the mouse to walk across an elevated narrow beam to a safe platform. This test takes place over one day, with

each mouse being given three trials. During the first trial, some animals may need encouragement (such as an occasional nudge with a finger) to traverse the full length of the beam. The time taken by the mouse to traverse the beam, the percentage of immobility, backward motion and drag walk and the number of paw slips and falls that occurred in the process were measured. The apparatus consisted of a 1-m smooth piece of wood and square in shape (9 mm wide), resting 50 cm above the tabletop on two narrow support stands to hold up the start section of the beam. A goal box with nesting material from home cages was placed at the end of the beam to attract the mouse to the finish point. A white led lamp (590 lm) was used as an aversive stimulus (bright light) to shine light above the start point (Brooks and Dunnett, 2009; Curzon et al., 2009).

2.2.6. Wire hang test

The mice were tested three times in one day. The structure was handmade using a 40-cm-long metal wire (2 mm diameter) held by two metal bars at a height of 50 cm. Each animal was placed on the middle of the wire and allowed to hang. The time it held on before releasing the wire was measured (Aartsma-Rus and van Putten, 2014). Animals that fell in <5 s were placed on the wire again. In the case of a full passive hold, the timer was stopped, and the previous data also recorded.

2.2.7. Morris water maze

The Morris water maze consisted of a circular pool (90 cm diameter and 60 cm high) made of light grey-colored plastic. The apparatus was filled with water (28 °C ± 2 °C) to a depth of 40 cm. Non-toxic tempera paint was used to render the water opaque. The pool was arbitrarily divided into four equally-sized quadrants, and four starting positions were assigned: North, South, East and West. The mice were tested for four consecutive days and were given four trials per day (starting from each of the four cardinal positions). The animals were then allowed to rest for three days before being tested again on day 8. On days 1–4 of training, a cylindrical non-colored platform made of plexiglass (80 mm in diameter) was placed in the North-East quadrant (not visible) just in line with the water surface. The escape latency to reach the hidden platform was measured. If the mice could not reach the platform within 60 s, they were gently led onto the platform and allowed to remain there for 10 s. The mice were then dried and returned to their cages to rest for at least 30 min before the next trial. On day 8, the platform was removed. The mice were given four trials (released from the four starting positions) and were allowed to swim for 60 s in order to determine their search patterns. Their swimming distance and speed, moving, still and/or floating time and the time spent, the distance and moving and still time in platform zone were measured (Bromley-Brits et al., 2011; Deacon, 2013b; Nunez, 2008).

2.3. Glucose and insulin tolerance tests

For the glucose tolerance test (GTT), the mice were fasted for 16 h, while for the insulin tolerance test (ITT), they were fasted for 4 h, followed by intraperitoneal injection of 2 g/kg glucose (D-(+)-Glucose, Sigma-Aldrich, Madrid) or 1 UI/kg insulin (Actrapid 100 UI/ml, Novo Nordisk Pharma S.A., Madrid), respectively. Blood samples were measured with an Accu-Chek Performa (Roche, Barcelona, Spain) before injection (time 0) and at 15, 30, 60, 90 and 120 min after injection (Benede-Ubieto et al., 2020).

2.4. Blood and serum parameters

For serum measurements, blood was collected by submandibular or cardiac puncture in BD Vacutainer® SST™ II Advance tubes (Fisher Scientific, Madrid, Spain). Serum was obtained after a centrifugation of 2000 *g*, 4 °C, 10 min (Greenfield, 2017; Parasuraman et al., 2010; Golde et al., 2005). Insulin was measured by Mercodia Ultrasensitive Mouse Insulin ELISA (Mercodia, Uppsala, Sweden), while a Mouse Leptin ELISA Kit (Invitrogen, Madrid, Spain) was used to measure leptin. The determination of triglycerides was carried out by an enzymatic-colorimetric assay with a Spinreact GPO-POD kit (Spinreact, Girona, Spain). Measurements were taken using a Multiskan™ GO Microplate Spectrophotometer (Thermo Scientific, Madrid, Spain) for ELISA and the enzymatic-colorimetric assay. A biochemical profile was obtained using the VetScan Comprehensive Diagnostic Profile reagent rotor used in a VetScan VS2 Chemistry Analyzer (Zoetis, Madrid, Spain). A volume of 120 μL of serum was required for the quantitative determinations.

Basal glucose was measured in duplicate throughout the life of the animal using blood samples from the tail with an Accu-Chek Performa (Roche, Barcelona, Spain).

2.5. Hematology analyses

Hematology analyses were carried out from whole blood collected by cardiac puncture in BD Vacutainer® K2EDTA or K3EDTA blood collection tubes (Fisher Scientific, Madrid, Spain). A total of 23 hematological parameters were obtained using a BC5000-Vet analyzer (Mindray, Madrid, Spain).

2.6. [^{18}F]-2-fluoro-2-deoxy-D-glucose by positron emission tomography with computed tomography

Prior to image acquisition, the animals were acclimatized for at least two days at the local animal facility. One day before the experiments, the mice were fasted overnight, for approximately 16 h. After this time, they were anesthetized with 3% isoflurane (Baxter, Madrid, Spain) for induction and 2.5% for maintenance and intravenous administration of 5.86 ± 0.54 MBq of [^{18}F]-2-fluoro-2-deoxy-D-glucose ([^{18}F]-FDG) (Galaria, Galicia, Spain) in a volume of 0.07–0.08 mL. This was administered via the tail vein. The animals were then awakened and placed back in their cages for 20 min before being anesthetized again and placed in prone position on the bed of the microPET scanner (Albira PET/CT Preclinical scanner, Bruker Biospin Corp. Billerica, MA, USA). Finally, the positron emission tomography (PET) and the computed tomography (CT, Standard Quality, 200 μA y 35 kV) were acquired 30 min after the radiotracer injection. The acquisition consisted of a 1-bed position PET scan (149 mm along axial direction) of 10 min and a 1-bed position CT scan (64 mm along axial direction) of 10 min duration.

PET data acquisitions were reconstructed using the maximum likelihood expectation maximization (MLEM) algorithm with 12 iterations and a pixel size of 0.25 × 0.25 × 0.25 mm^3 using Bruker Albira Suite Software Version 5.0 (Billerica, Massachusetts, USA). For the image analysis, PET images were manually fused to CT images and PET/CT images were spatially normalized to a specific mouse T2 MRI Template (Ma-Benveniste-Mirrione mouse brain) by rigid transformation using PMOD v4.2 software (PMOD Technologies, Zürich, Switzerland) (Mirrione et al., 2007; Ma et al., 2005). Mean radioactivity concentrations were estimated in each predefined volume of interest (VOIs) of the VOI template Ma-Benveniste-MirrioneMouse. Subsequently, mean standardized uptake values (SUV_{mean}) were calculated by normalizing the radioactivity concentration by the injected dose (MBq) and the body weight (Kg) of each mouse as follows:

2.7. Histology

2.7.1. Tissue processing

Tissues were fixed in 4% m/v neutral buffered formalin and paraffin-embedded (L, 2014). Cerebellum, cerebral cortex, striatum, hypothalamus, hippocampus, mesencephalon, liver and white and brown fat were sectioned at a thickness of 4 μm and stained with hematoxylin and eosin (H&E). Immunodetection was performed for the cerebellum, cerebral cortex, striatum, hypothalamus, hippocampus and mesencephalon with anti-ubiquitin (Ubi-1, cat# ab7254, Abcam; Cambridge, UK; Citrate Buffer (BC), 1:1000, overnight, 4 °C), Glial fibrillary acidic protein

(GFAP, cat# IR524, Agilenet Dako, Madrid, Spain Tris-EDTA buffer (TE), ready-to-use (RTU), 30 min, room temperature (RT)) and Cluster of Differentiation 68 (CD68, cat# ab125212, Abcam, Cambridge, UK; BC, 1:1.000, overnight, 4 °C) antibodies.

2.7.2. Imaging

Samples were visualized with an Olympus BX43 microscope (Olympus Corporation) and photographed with an Olympus DP72 digital camera using the cellSens software (Olympus Corporation).

2.7.3. Total non-alcoholic fatty liver disease activity score

The H&E liver sections were scored blindly by two experienced pathologists using the Nonalcoholic Steatohepatitis Clinical Research Network (NASH CRN) criteria (Kleiner et al., 2005). NAS ranged from 0 to 8, which was calculated by a sum of scores of steatosis (0–3), lobular inflammation (0–3), and ballooning degeneration (0–2).

2.8. RNA isolation and quantitative real-time PCR

Total RNA was extracted from brain tissue (cerebellum, midbrain, hypothalamus, cortex, hippocampus, striatum) using TRI Reagent® (cat# TR 118, Molecular Research Center (MRC), Ohio, USA) and ReliaPrep™ RNA Tissue Miniprep System (cat# Z6112, Promega, Madrid, Spain) as per the manufacturers' instructions. RNA was reverse-transcribed using an M-MLV Reverse transcriptase kit (Invitrogen, Madrid, Spain), as previously described (Victoria et al., 2010).

Specific primers and probes designed by the Universal ProbeLibrary (Roche Diagnostics, Sant Cugat del Valles, Spain) were used in a Light Cycler 2.0 (Roche Diagnostics) to determine the expression of the *Gng3* gene (Table 1). Real-time qPCR analyses were performed in duplicate. A QuantStudio™ 5 Real-Time PCR System (Applied Biosystems, Madrid, Spain) was used to specifically determine the expression of the following genes: *Bscl2*, Celia *BSCL2*-TG, *Pparg*, *Pex16*, *Sod1*, *Sod2*, *Cat*, *Pex11g*, *Gpx1*. Specific primers and probes were designed with the Primer3Plus software (http://www.bioinformatics.nl/cgi-bin/primer3plus/primer3plus.cgi) or the TaqMan Assay Search Wizard guide (Applied Biosystems, Madrid, Spain) (Table 1). Specifically designed primers and probe were used for the *BSCL2* spliced transcript. Real-time qPCR analyses were performed in triplicate. Real-time PCR conditions are available upon request. Results were normalized to the *Rn18S* gene using the $2^{-\Delta\Delta\ CT}$ method (Livak and Schmittgen, 2001).

2.9. Western blotting

Protein extracts from brain areas (cerebellum, midbrain, hypothalamus, cortex, hippocampus and striatum) were isolated from the phenol-ethanol supernatant obtained after precipitation of DNA with ethanol in the RNA extraction procedure with TRI Reagent (see Protocol S1) and protein content was determined via Bradford protein assay. Protein samples were transferred to a PVDF transfer membrane (Amersham Hybond PVDF 0.45 μm, Cytiva, Vienna, Austria). Blots were blocked for 25 min at room temperature in 2% or 5% fat-free milk powder (TBS, Tween-20 0.1%). Incubation with primary antibodies was performed overnight at 4 °C. The blots were probed with anti-6xhis-tag dilution 1:1000 (MA1–21315, Thermo Scientific, Madrid, Spain). Anti-GAPDH dilution 1:25,000 (G9545, Sigma-Aldrich, Madrid, Spain) was used as loading control. Conjugated peroxidase anti-mouse IgG (ab6789, Abcam, Cambridge, UK) or conjugated peroxidase anti-rabbit IgG (A16104, Fisher Scientific, Madrid, Spain) were the secondary antibodies, dilution 1:5000 and 1:10,000 respectively. Bands were revealed by chemiluminescence with the Immobilon Forte Western HRP Substrate (Millipore, ref. WBLUF0100).

2.10. Statistical analysis

Statistical significance was determined using the non-parametric Kruskal-Wallis test, followed by a post-hoc Mann-Whitney U. Data are presented as mean ± SD with statistical significance set at $p < 0.05$. All statistical analyses were performed using IBM SPSS Statistics (release 25.0; SPSS, Chicago, IL, USA).

3. Results

3.1. BSCL2-associated Celia's encephalopathy murine model

A novel PELD mouse model has been generated by the insertion of human Celia *BSCL2*-TG using a strategy based on the Cre/loxP recombination system (as described in Fig. 1). The transgene sequence was corroborated by sequencing and the genotype was examined by PCR (data not shown). Normal expression of *Gng3* (data not shown), an adjacent gene to *Bscl2* (Fig. 1), was also detected, thus confirming that transgene insertion does not affect the expression of this gene. As the homozygous *Bscl2*$^{Celia/Celia}$ male mice were sterile (data not shown), the colony was maintained by crossing heterozygous *Bscl2*$^{+/Celia}$ mice. Genotypes followed a Mendelian pattern (24.3% wild type (n = 132), 24.7% *Bscl2*$^{Celia/Celia}$ (n = 134), 51.0% *Bscl2*$^{+/Celia}$ (n = 277)) (Fig. 2). The male to female ratio was 47.7:52.3% in wild type, 53.8:46.2% in *Bscl2*$^{+/Celia}$ and 44.8:55.2% in *Bscl2*$^{Celia/Celia}$.

3.2. Adipose tissue and liver findings

On dissection, *Bscl2*$^{Celia/Celia}$ mice displayed a near-total absence of fat, affecting both white (WAT) and brown fat (BAT) (interscapular BAT, inguinal WAT, gonadal WAT), representing a severe lipoatrophic phenotype (Fig. 3a-b). Histology of residual brown fat showed adipocytes with larger lipid vacuoles and areas of necrosis, while white fat presented smaller adipocytes and areas of fibrosis. Both cases showed lymphocyte infiltrates (Fig. 3c). On the other hand, normal fat depots were observed in both wild type and heterozygous mice. The liver of these homozygous mice was enlarged as a consequence of ectopic fat

Table 1
Primer sequences and probes used for qPCR analysis.

Gene	Forward primer (5′-3′)	Reverse primer (5′-3′)	Probe sequence (5′-3′)
Gng3	TCCATCCGTTCAGGCAAT	TCTTCAAATGCCTTTACCTTTCA	CCTGGAGC
Rn18s	AAACGGCTACCACATCCAAG	TACAGGGCCTCGAAAGAGTC	CGCAAATTACCCACTCCCGACCCG
Bscl2	CCAAGGGTATCGTCCCTGT	GGGACTGGTGGGTCATTG	TTCCTGGC
Celia *BSCL2*-TG	GTATCGTCCCTGTGGAAGAC	TAGAGTGATGGTGATGGTGATG	AGCCAGGAACTCAAAGCCTGAGG
Pparg	CTTGACAGGAAAGACAACGG	TGGCACCCTTGAAAAATTCG	GCAGGAGCAGAGCAAAGAGGTGGCC
Pex16	TATGTGACTCGTCATCCAGC	AGTACACCAGTTCAGACAGC	ACGGCTGTGCGGGGCCTCAGTT
Sod1	TGGGGACAATACACAAGGC	CTTTCCAGCAGTCACATTGC	TGGCCCGGCGGATGAAGAGAGGCA
Sod2	GCACTGAAGTTCAATGGTGG	CAAAGTCACGCTTGATAGCC	ACCTGAGCCCTAAGGGTGGTGGAGA
Cat	GTCTCTCCATCAGGTTTC	CTGGTCGGTCTTGTAATG	CAATAGACTGCCTCTCCATCTGC
Pex11g	GTGACTGACCAACTGTACTA	CACAGGGCCTTGACAG	CCTTGTGAGCATATCGCCTGG
Gpx1	GATGAACGATCTGCAGAAGC	CATTCTTGCCATTCTCCTGG	ACCTCGTGGACTGGTGGTGCTCGGT

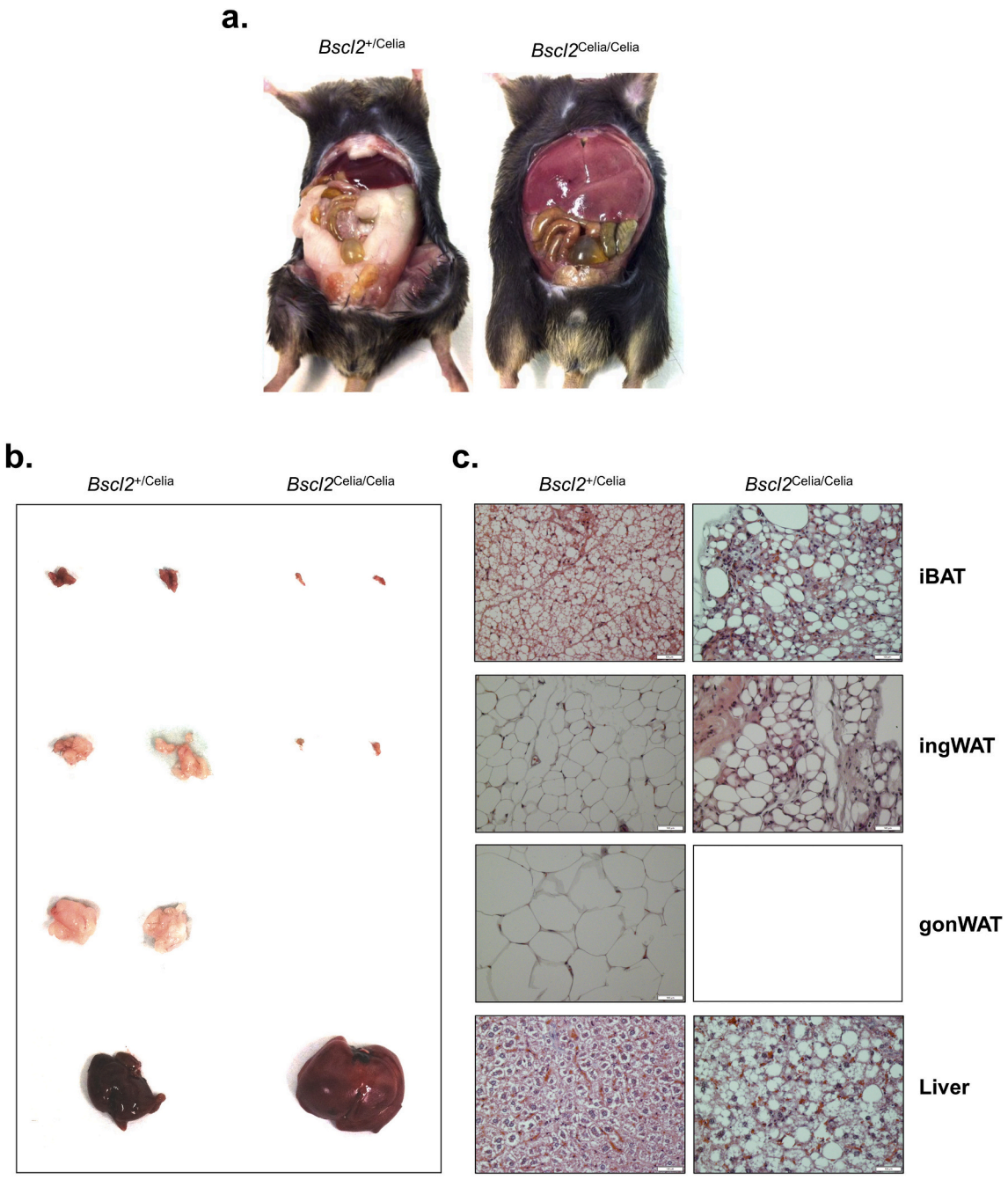

Fig. 3. a. Dissection of the trunk area of both *Bscl2*$^{+/Celia}$ and *Bscl2*$^{Celia/Celia}$ mice (6.1 months old). b and c. Macroscopic appearances (b) and histology (c) of interscapular brown adipose tissue (iBAT), inguinal white adipose tissue (ingWAT), gonadal white adipose tissue (gonWAT) and liver of 6.1-month-old *Bscl2*$^{+/Celia}$ and *Bscl2*$^{Celia/Celia}$ mice. Scale bar: 100 μm. (For interpretation of the references to colour in this figure legend, the reader is referred to the web version of this article.)

deposition with histological signs of hepatic steatosis (Fig. 3c, Fig. 9a-b), representing in some cases, 25% of the weight of the animal (Fig. 4c, Fig. 3a-b and see Fig. S1d). This disorder started early and got worse over time. However, homozygous, severely neurologically affected animals presented mild steatosis (Fig. 9a-b) and the size of their liver was much smaller compared to the non-severely affected homozygous animals, being more similar to non-severely affected heterozygous mice. These homozygous mice also had enlarged visceral organs (liver, heart, kidneys and spleen) and a similar weight (Fig. 4b-c, see Fig. S1d), despite showing an almost total absence of fat, compared to wild type and heterozygous animals.

3.3. Glucose metabolism and analytical findings

Metabolic parameters of wild type, *Bscl2*$^{+/Celia}$, *Bscl2*$^{Celia/Celia}$ and severely affected (S.A.) mice were examined in fasting states. The *Bscl2*$^{Celia/Celia}$ mice used in the present study showed severe hyperinsulinemia and hypoleptinemia (Fig. 5a-b). On the other hand, serum triglycerides levels were significantly lower compared to wild type and *Bscl2*$^{+/Celia}$ at 4 months of age, although no differences among phenotypes were found at 9.5 months (Fig. 5c). For S.A. mice, this metabolic pattern was altered, despite presenting hypoleptinemia, and a lack of hyperinsulinemia. However, a pattern of increase was observed, which was not statistically significant, perhaps due to the small number of

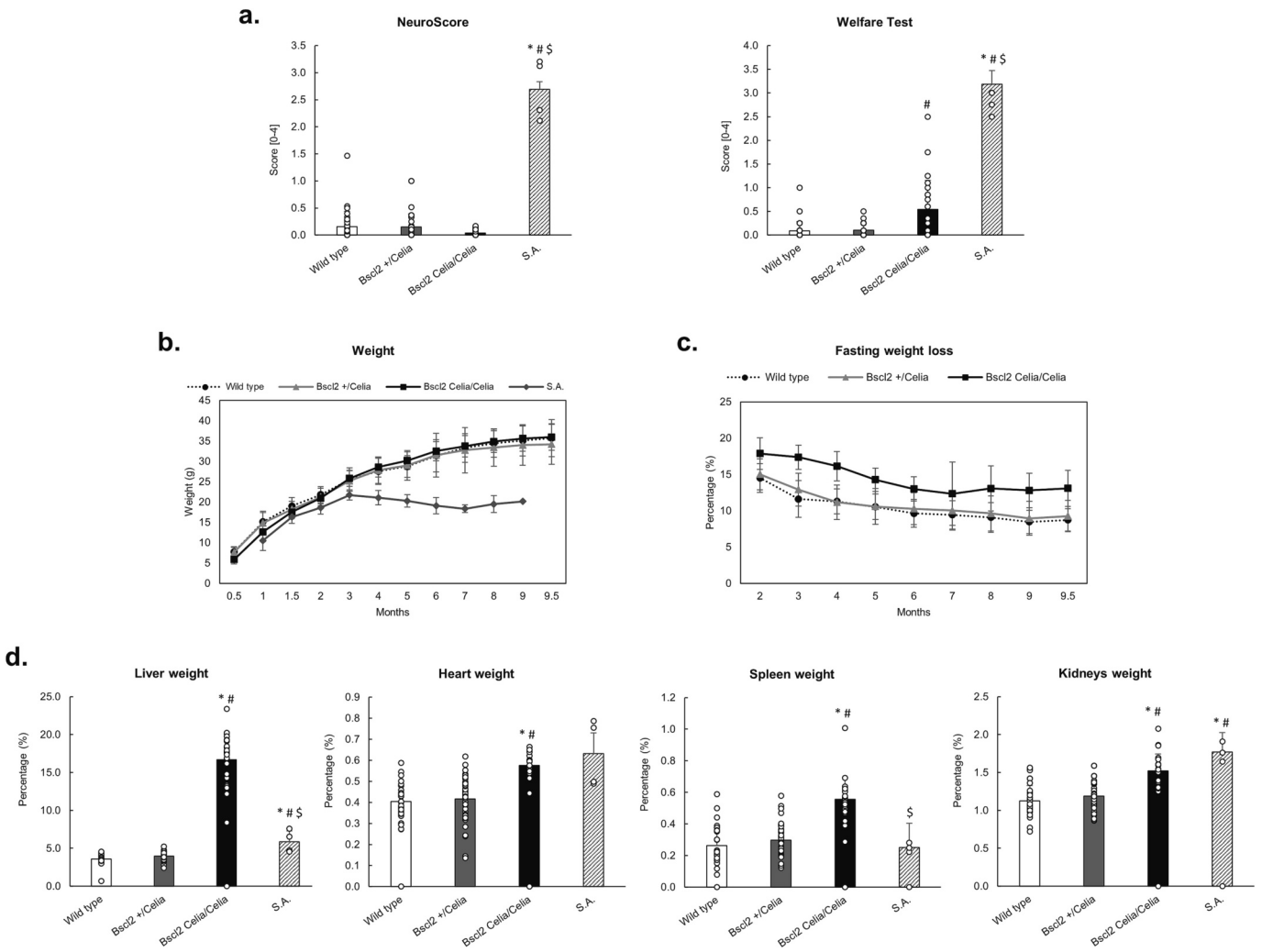

Fig. 4. Phenotypic comparison. a. NeuroScore and Welfare test from 32 wild type, 37 *Bscl2*$^{+/Celia}$, 25 *Bscl2*$^{Celia/Celia}$ and 4 severely affected animals. Mean age 7.5 months. b. Weight evolution from 0.5 to 9.5 months (85 wild type, 106 *Bscl2*$^{+/Celia}$, 53 *Bscl2*$^{Celia/Celia}$ and 11 severely affected). c. Evolution of the percentage of weight loss after fasting from 2 to 9.5 months. Wild type, $n = 29$; *Bscl2*$^{+/Celia}$, $n = 40$ and *Bscl2*$^{Celia/Celia}$, $n = 27$ d. Organ weight (liver, heart, spleen and kidneys). Mean age 9.5 months for the 33 wild type, 43 *Bscl2*$^{+/Celia}$ and 24 *Bscl2*$^{Celia/Celia}$ and 7.7 months for the 4 severely affected animals. Data is presented as mean ± SD. Statistics: non-parametric Kruskal-Wallis test, followed by a post-hoc Mann-Whitney U. * $p < 0.05$ vs wild type; $^{\#}$ $p < 0.05$ vs *Bscl2*$^{+/Celia}$; $^{\$}$ $p < 0.05$ vs *Bscl2*$^{Celia/Celia}$.

animals. It should also be noted that these animals did not show an increase in serum triglyceride concentration over time as was the case with *Bscl2*$^{Celia/Celia}$ (Fig. 5a-c). To complete the metabolic profile of our knock-in mice, both a hematological (see Table S1) and biochemical profile (see Table S2) were created. No differences in creatinine values were present between the genotypes, while alanine aminotransferase and alkaline phosphatase showed a significantly higher concentration in *Bscl2*$^{Celia/Celia}$ mice compared to wild type and *Bscl2*$^{+/Celia}$. In this case, only one S.A. mouse could be analyzed due to the necessary volume required. However, values similar to those of wild type and *Bscl2*$^{+/Celia}$ mice were suggested (Fig. 5d-f). Glucose tolerance and insulin resistance were evaluated in wild type, *Bscl2*$^{+/Celia}$ and *Bscl2*$^{Celia/Celia}$ at 3 and 3.5 months of age. The GTT showed no impairment of glucose metabolism in *Bscl2*$^{Celia/Celia}$, displaying the same pattern in all the genotypes, while the ITT showed that *Bscl2*$^{Celia/Celia}$ had reduced insulin sensitivity compared with both wild type and *Bscl2*$^{+/Celia}$ (Fig. 5h-i). Basal glucose was also monitored throughout the life of the animals, showing high levels in *Bscl2*$^{Celia/Celia}$ animals (Fig. 5g, see Table S2). For the results of GTT, ITT and basal glucose separated by sex, see Fig. S2.

3.3.1. Neurological clinical phenotype

A total of 31 mice developed severe neurological alterations, of which 16 (11.9%) were *Bscl2*$^{Celia/Celia}$ mice, and 15 (5.4%) *Bscl2*$^{+/Celia}$ mice. Within the percentage of S.A. homozygous animals, 6.0% were female and 6.0% were male, while in heterozygous animals this percentage was 2.2% and 3.2%, respectively. Neurological signs began to appear at approximately 5 months of age and became more evident throughout the life of the animal, which was severely reduced (8.4 months). Ponderal stagnation, abnormal crossing of the limbs, kyphosis, tremor or myoclonus, tail spasticity and paraparesis or paraplegia (Fig. 6a and see Video S1) constitute the most recurrent neurological involvement in these S.A. mice. This neurological phenotype was corroborated by the NeuroScore and Welfare tests performed at 7.5 months of life, which showed up to 20 times more severity compared to mice that did not develop symptoms of neurodegeneration (Fig. 4a, see Fig. S1a). Observation of the animals' nesting behavior made it possible to evaluate their levels of distress (Gaskill et al., 2013). Thus, it was confirmed that the non-S.A. homozygous animals presented worse nests and, therefore, greater distress than wild type mice (Fig. 6b). The nest evaluation of S.A. mice was not possible due to the impossibility of separating them into isolated boxes, which would have caused them

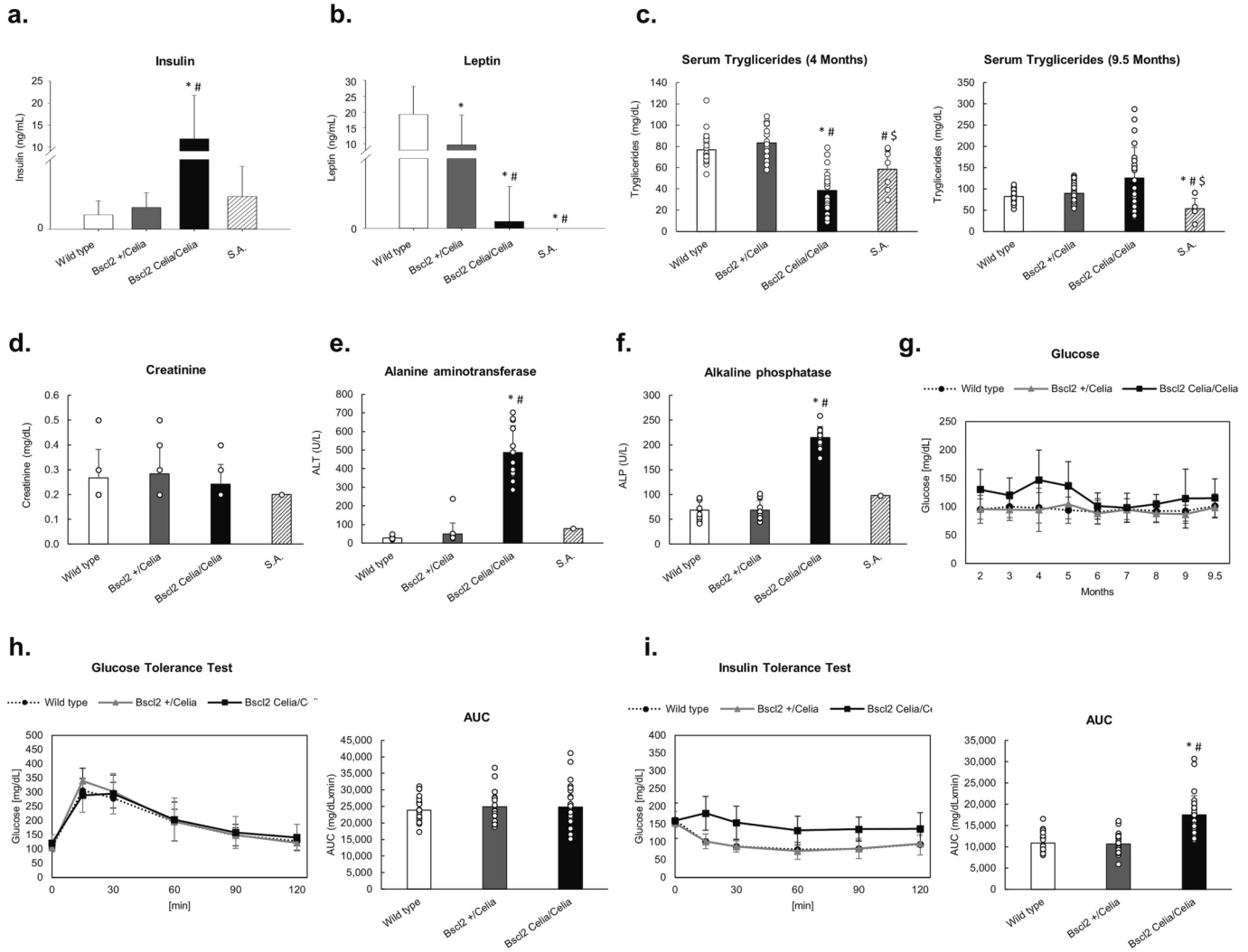

Fig. 5. Metabolic measurements for wild type, *Bscl2*$^{+/Celia}$ and *Bscl2*$^{Celia/Celia}$ animals. Insulin (a), leptin (b), triglyceride concentration at 4 and 9.5 months (c), creatinine (d), alanine aminotransferase (e) and alkaline phosphatase (f) were measured in serum. Basal glucose evolution from 2 to 9.5 months (29 wild type, 39 *Bscl2*$^{+/Celia}$ and 26 *Bscl2*$^{Celia/Celia}$) (g). Glucose tolerance test (h) and insulin tolerance test (i) were measured as evolution of glucose concentration (mg/dL) over time and area under the curve (AUC). $n = 23$ wild type, $n = 20$ *Bscl2*$^{+/Celia}$ and $n = 29$ *Bscl2*$^{Celia/Celia}$. Mean age 3 and 3.5 months, respectively. For mean age and number of animals per genotype see Table S4. Data is presented as mean ± SD. Statistics: non-parametric Kruskal-Wallis test, followed by a post-hoc Mann-Whitney U. * $p < 0.05$ vs wild type; $^{\#}$ $p < 0.05$ vs *Bscl2*$^{+/Celia}$; $^{\$}$ $p < 0.05$ vs *Bscl2*$^{Celia/Celia}$.

greater discomfort. In addition, due to this neurological profile, the S.A. animals also showed a reduction in weight (Fig. 4b, see Fig. S1b). No differences were found in severity of weight loss between S.A. heterozygous and S.A. homozygous mice.

The transgenic murine model for Celia seipin and wild type mice was evaluated for possible sensorimotor derangement (see Table S3). In the open field and elevated zero maze tests, the non-S.A. *Bscl2*$^{Celia/Celia}$ animals showed a decrease in locomotor activities and greater anxiety compared to the wild type and *Bscl2*$^{+/Celia}$ animals (Fig. 7a-b). In addition, the beam walking test clearly showed less coordination and balance in these animals (Fig. 7c). Furthermore, the Morris water maze showed less distance travelled and slower speed, which are indicative of a decrease in the motor activity of these *Bscl2*$^{Celia/Celia}$ animals (Fig. 7d). However, this was not the case in parameters relating to cognitive functions and memory. The other behavioral studies performed (rotarod test and wire hang test) did not show significant differences between genotypes. However, due to their physical discomfort, S.A. animals could only be included in the tests implying the lowest levels of stress (open field and elevated zero maze).

3.3.2. Brain PET

[^{18}F]-FDG PET/CT images were obtained for six wild type, six *Bscl2*$^{Celia/Celia}$ and two S.A. *Bscl2*$^{Celia/Celia}$ mice (Fig. 8). Although no statistical analysis could be carried out due to the sample size, the data show a decrease in brain [^{18}F]-FDG uptake in S.A. mice compared to wild type (26% global reduction) at 8.4 months, while a global reduction of 5% was observed when compared to non-S.A. *Bscl2*$^{Celia/Celia}$ (Fig. 8c). However, this reduction was not clear at 4.3 months. Fig. 8b shows SUV_{mean} values of each analyzed VOI for the three groups. The greatest changes in S.A. animals, when compared with wild type and non-S.A. *Bscl2*$^{Celia/Celia}$ animals, respectively, were observed in brain regions such as the olfactory bulb (34% and 16% reduction), cortex (36% and 13% reduction), amygdala (31% and 15% reduction) and left striatum (27% and 9% reduction) at 8.4 months (Fig. 8c). Furthermore, brain PET images of all the animals can be observed in Fig. 8a, in which the reduction of [^{18}F]-FDG brain uptake can be visually appreciated in the S.A. ($n = 2$) and non-S.A. *Bscl2*$^{Celia/Celia}$ ($n = 6$) mice compared to wild type animals (n = 6).

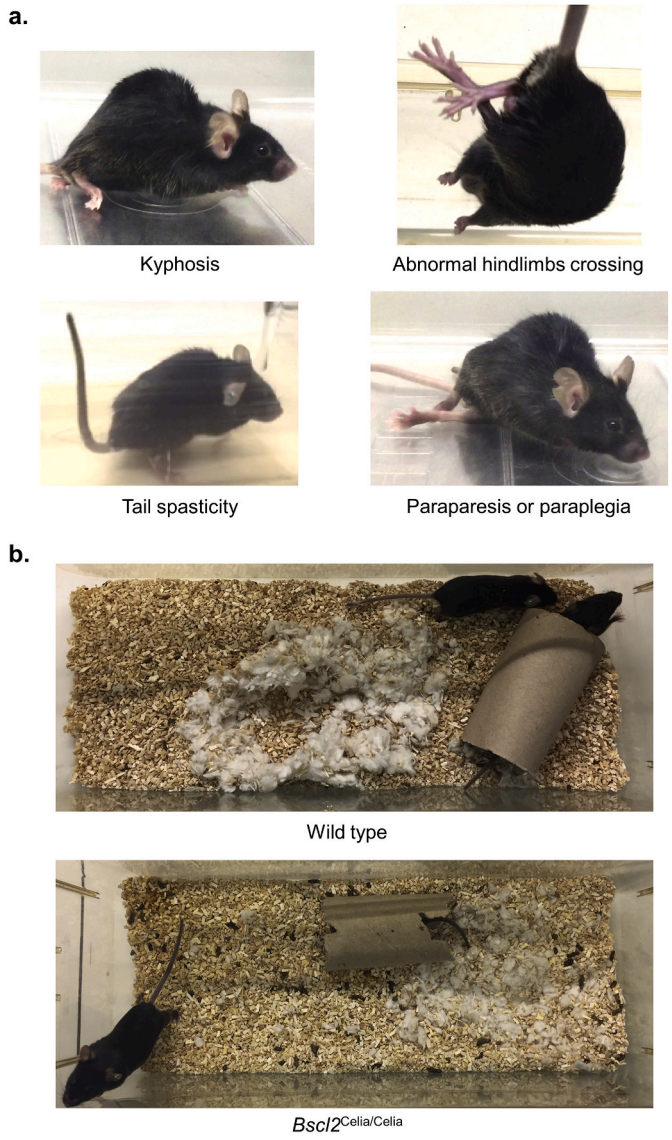

Fig. 6. a. Neurological signs of severely affected animals. Kyphosis, abnormal hindlimb crossing, tail spasticity and paraparesis or paraplegia. b. Wild type and non-severely affected *Bscl2*$^{Celia/Celia}$ nest building.

3.3.3. Brain histology

Histological studies of hematoxylin-eosin-stained sections of the cerebellum showed a moderate patchy loss of Purkinje cells (functional units involved in motor coordination) in 30% of S.A. animals. In these animals, on ubiquitin immunostaining, Purkinje cells were surrounded by groups of distinct glial cells with a prominent nucleolus. No evident ubiquitin-reactive intranuclear inclusions were observed at this or other levels. These cells were present in areas still containing Purkinje cells, with their location suggesting that they could correspond to Bergmann's astrocytes. In addition, the deep cerebellar layer contained occasional grain cell nuclei with a prominent nucleolus (Fig. 9c). In both cell types, the presence of ubiquitin-reactive nuclear inclusions cannot be ruled out. Neurologically unaffected animals presented normal cerebellar histology (wild type ($n = 3$, 7.8 months); *Bscl2*$^{+/Celia}$ ($n = 1$, 7.4 months); *Bscl2*$^{Celia/Celia}$ (n = 3, 8.7 months)) (data not shown). No other differences were disclosed in ubiquitin immunostaining of the cerebral cortex, striatum, hypothalamus, hippocampus or mesencephalon. No differences were found for GFAP and CD68 staining.

3.3.4. qPCR

Real time PCR studies were carried out to determine the expression of the Celia *BSCL2* transgene, *Bscl2* wild type and mitochondrial and peroxisome genes. As expected, wild type animals did not show expression of the human transgene (Celia *BSCL2*-TG) but of the wild type *Bscl2* (Fig. 10a-b, see Table S4). Regarding the expression of this transgene in KI mice, this was significantly higher in non-S.A. homozygous mice in the cerebellum (Δ131%), hypothalamus (Δ240%), cortex (Δ75%) and striatum (Δ197%) (Fig. 10b, see Table S4), when compared with non-S.A. heterozygous animals. However, no differences were found in the midbrain and hippocampus. Celia *BSCL2* transgene expression in S.A. homozygous mice was significantly higher than heterozygous animals in the midbrain, hippocampus and striatum (Δ157–284%) and cortex (Δ245%). In the latter area, the human transgene was overexpressed Δ97% when it was compared with non-S.A. *Bscl2*$^{Celia/Celia}$ (Fig. 10b, see Table S4). On the other hand, the expression of the human transgene in S.A. heterozygous mice was no different than in non-S.A. heterozygous animals. However, there was a lower expression of *Bscl2* wild type in S.A. heterozygous compared to non-S.A. mice in tissues such as the cerebellum (Fig. 10a).

Regarding the expression of the other analyzed genes, no differences were found for *Pparg*, *Pex16*, *Cat* and *Gpx1* (see Table S4).

The expression of the mitochondrial *Sod2* gene was significantly reduced in striatum in both S.A. homozygous and heterozygous mice (−Δ57% and -Δ68%, respectively) (Fig. 10d, see Table S4). *Sod1* gene expression in the cortex was also reduced in both homozygous and heterozygous S.A. mice (−Δ42% and -Δ51%, respectively), although the differences were not statistically significant. On the other hand, the expression of this gene (*Sod1*) was 163% significantly higher in the midbrain of S.A. *Bscl2*$^{+/Celia}$ mice compared with the other genotypes (Fig. 10c, see Table S4). Furthermore, the *Pex11g* gene showed an increased expression in the hypothalamus of S.A. compared to wild type animals, as was the case with unaffected homozygous and heterozygous animals (Fig. 10e, see Table S4).

3.3.5. Western blot

Due to the lack of a specific antibody anti-Celia-Seipin, the amount of this aberrant human protein was analyzed in several non-affected KI murine brain areas by Western blot using 6×His-tagged Celia seipin. The theoretical weight of Celia seipin with 6× His tag was 40.25 kDa (39.43 kDa + 0.84 kDa, respectively). In both genotypes, heterozygous and homozygous, obvious bands were only observed in the cortex, hypothalamus and hippocampus, but no signal was detected in the cerebellum, midbrain and striatum compared to the hypothalamus of a human without the disease (Fig. 10f).

4. Discussion

In this study, a humanized KI mouse has been generated which partially recapitulates PELD. The neurologically affected mice showed many of the clinical features which appear in human beings suffering from this devastating disorder. Thus, these mice showed severe neurological symptoms early in life and their life expectancy was dramatically reduced. Affected animals, as in the case with humans, presented myoclonus, spasticity and paraparesis or paraplegia, dying as a consequence of a severe encephalopathic condition (Guillen-Navarro et al., 2013; Sánchez-Iglesias et al., 2021). Also, as in humans (Guillen-Navarro et al., 2013; Araujo-Vilar et al., 2018), affected animals showed a reduction of brain glucose uptake in PET, as well as patchy loss of Purkinje cells and distinct glial cells with a prominent nucleolus that could correspond to Bergmann's astrocytes, and in both cell types the presence of ubiquitin-reactive nuclear inclusions cannot be ruled out. Regarding adipose tissue and hepatic phenotype, as occurs in some humans with the classical variant in homozygosity (Guillen-Navarro et al., 2013; Sánchez-Iglesias et al., 2021), homozygous affected mice presented severe generalized lipodystrophy and mild hepatic steatosis,

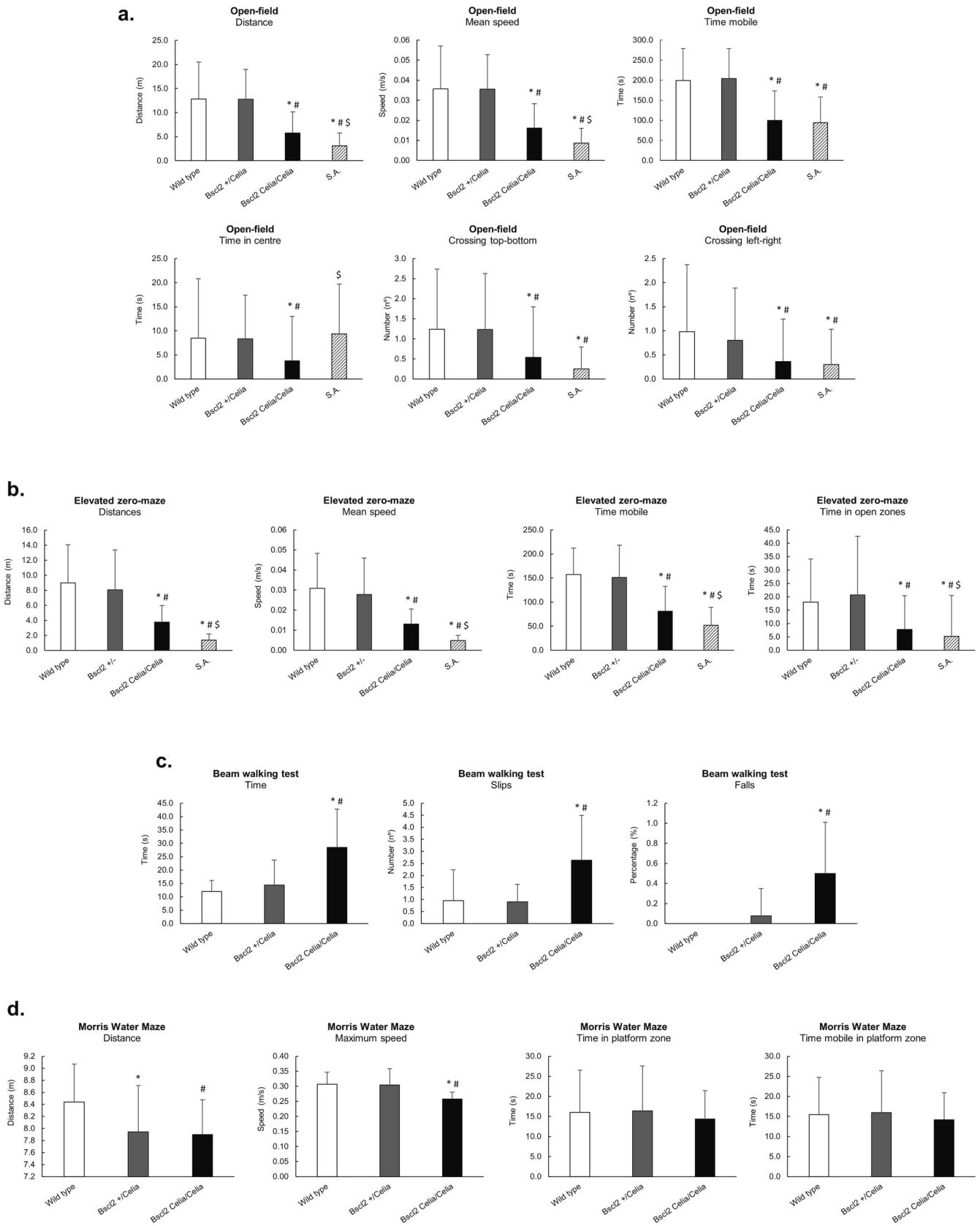

Fig. 7. Behavioral test analysis: a. Open field; b. Elevated zero maze; c. Beam walking test and d. Morris water maze for wild type, *Bscl2*$^{+/Celia}$, *Bscl2*$^{Celia/Celia}$ and severely affected (S.A.) mice. For mean age and number of animals per genotype see Fig. S1. Data is presented as mean ± SD. Statistics: non-parametric Kruskal-Wallis test, followed by a post-hoc Mann-Whitney U. * $p < 0.05$ vs wild type; $^{\#}$ $p < 0.05$ vs *Bscl2*$^{+/Celia}$; $^{\$}$ $p < 0.05$ vs *Bscl2*$^{Celia/Celia}$.

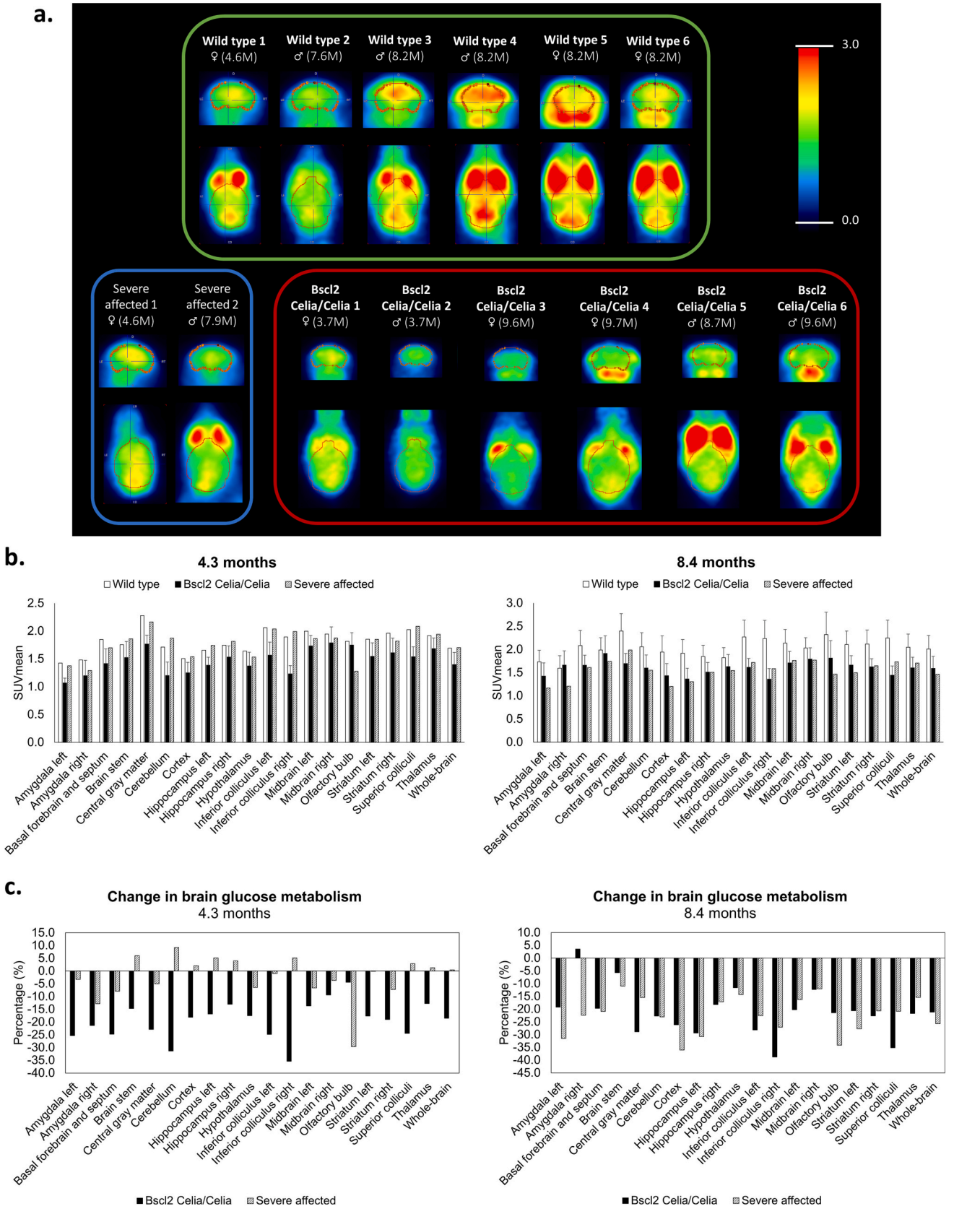

Fig. 8. Brain [^{18}F]-2-fluoro-2-deoxy-D-glucose by positron emission tomography with computed tomography comparing severely affected *Bscl2*$^{Celia/Celia}$ (n = 2) with wild type ($n = 6$) and non-severely affected *Bscl2*$^{Celia/Celia}$ (n = 6) animals. Brain PET images (a), mean standardized uptake value (SUV_{mean}) for 4.3 and 8.4 months (b) and mean % of change related to wild type animals for 4.3 and 8.4 months (c). Data is presented as mean ± SD.

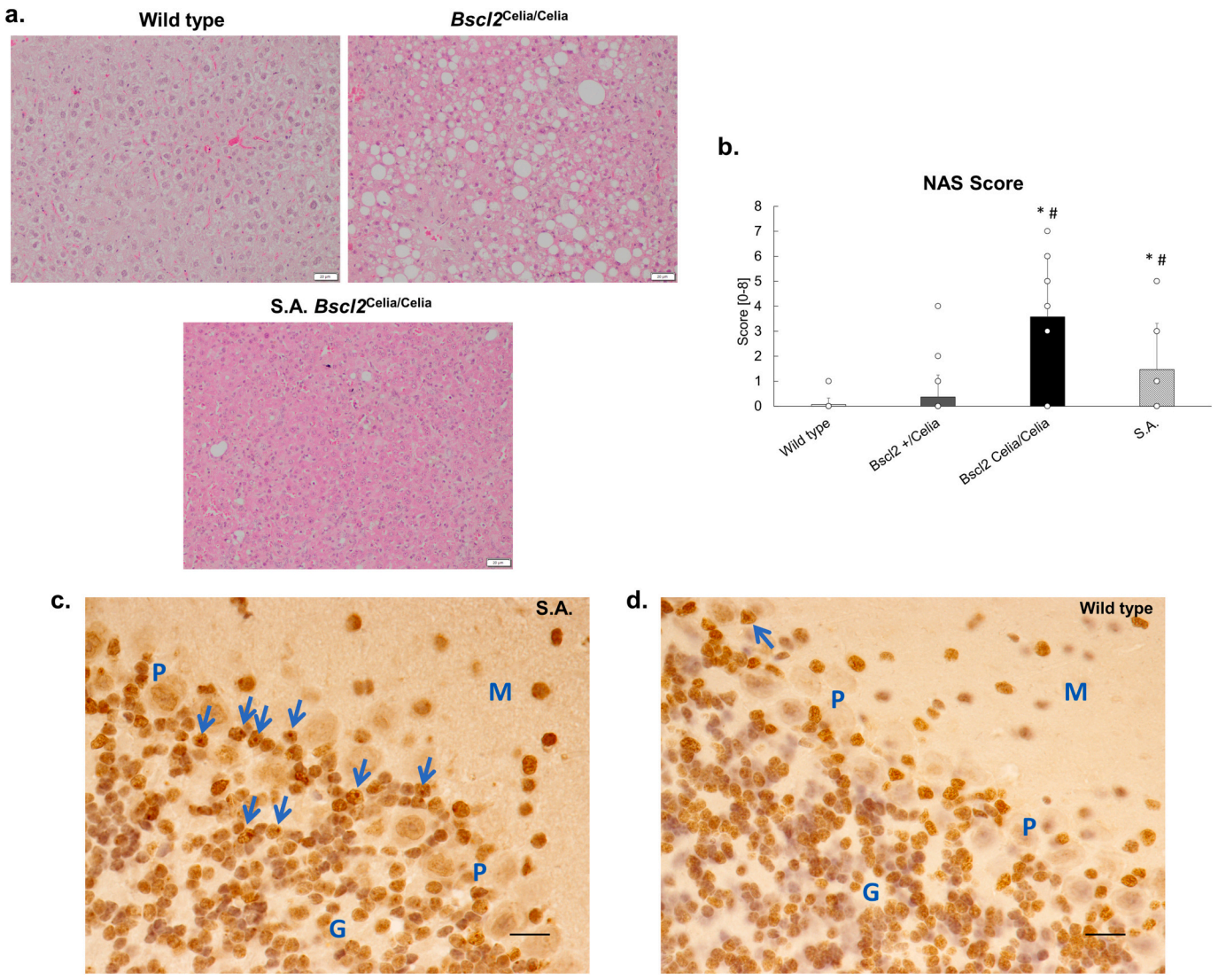

Fig. 9. a. Liver histology of 12-month-old wild type, 14-month-old *Bscl2*$^{Celia/Celia}$ and 19-month-old severely affected *Bscl2*$^{Celia/Celia}$ mice. Scale bar: 20 μm. b. NAS Score for wild type (n = 29; 3.3 months), *Bscl2*$^{+/Celia}$ ($n = 27$; 11.3 months), *Bscl2*$^{Celia/Celia}$ ($n = 21$; 10.6 months) and severely affected ($n = 13$; 9.1 months) animals. Data is presented as mean ± SD. Statistics: non-parametric Kruskal-Wallis test, followed by a post-hoc Mann-Whitney U. * $p < 0.05$ vs wild type; $^{\#}$ $p < 0.05$ vs *Bscl2*$^{+/Celia}$. c. High magnification microphotography of the Purkinje cell layer of a severely affected animal (S.A.) showing preserved Purkinje neurons with surrounding nuclei containing prominent nucleoli (arrows). These cells most probably correspond to Bergmann astrocytes. Note that some underlying grain cell nuclei also contain prominent dot-like nucleoli (arrows). In both cell types, the presence of ubiquitin-reactive nuclear inclusions cannot be ruled out. d. Similar microphotography of the cerebellar cortex Purkinje cell layer of a wild type animal with preserved Purkinje cells and only occasional nuclei displaying prominent nucleoli (arrow). M: molecular layer; P: Purkinje cell layer; G: granular layer. Scale bar: 20 μm.

while serum triglycerides and glucose metabolism were normal, without insulin resistance.

Despite the remarkable similarities between this murine model and PELD in humans, some important differences were found, and striking findings made. First of all, only 11.9% of homozygous KI mice exhibited obvious neurodegeneration. In human beings, all subjects carrying the classical variant c.985C > T, either in homozygosity or in compound heterozygosity, present a severe encephalopathic picture with a fatal outcome (Guillen-Navarro et al., 2013; Sánchez-Iglesias et al., 2021; Alaei et al., 2016; Poisson et al., 2019). Although it is also true that some other cases, due to another *BSCL2* variant (c.974dupG), which also leads to the skipping of exon 7 (Sánchez-Iglesias et al., 2021), only presented a mild neurological disorder (Sanchez-Iglesias et al., 2019b; Wu et al., 2009; Huang et al., 2010), these represent a minority and were frequently very young patients. At present, no obvious explanation exists for this finding. It is appealing to attribute more severe brain damage to a higher human transgene expression in the affected mice, which was only seen in the cortex, in which, on the other hand, glucose uptake was reduced. However, this does not explain the fact that 5.4% of heterozygous mice also showed a severe encephalopathic phenotype, in which the expression of Celia *BSCL2*-TG was similar to that of non-affected heterozygous animals. Although it has been reported that one *BSCL2* monoallelic variant (c.566 T > A) could be related with a profound refractory epilepsy and neurological regression (Fernandez-Marmiesse et al., 2019), this variant does not affect exon 7 and all the parents of PELD patients were fundamentally healthy. Having said this, and in view of these results, it cannot be ruled out that, at least in the murine brain and in a few cases, Celia *BSCL2*-TG in heterozygosity damages the brain. It must be taken into consideration that a mechanism of loss of seipin function has been assumed in congenital generalized lipodystrophy type 2. However, when explaining the pathogenic mechanism that produces neurodegeneration in PELD, it could be concluded that this damage is caused by a toxic gain of function. Some years ago, our group (Ruiz-Riquelme et al., 2015a) demonstrated in vitro that the

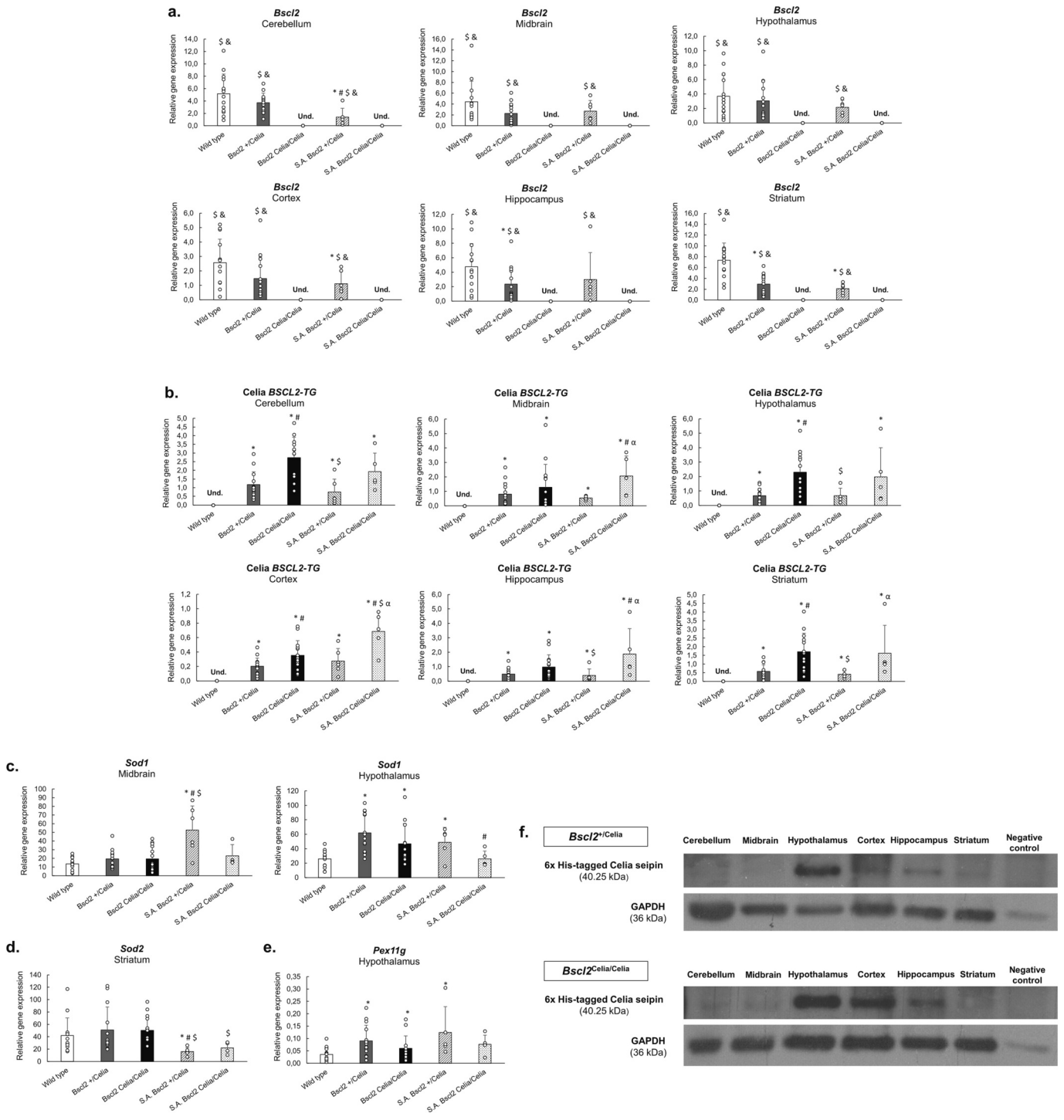

Fig. 10. Relative expression of (a) *Bscl2* and (b) Celia *BSCL2*-TG in the cerebellum, midbrain, hypothalamus, cortex, hippocampus and striatum; (c) *Sod1* in the midbrain and hypothalamus; (d) *Sod2* in the striatum and (e) *Pex11g* in the hypothalamus from 14 wild type (9.5 months), 14 $Bscl2^{+/Celia}$ (9.6 months), 14 $Bscl2^{Celia/Celia}$ (9.4 months), 5 severely affected $Bscl2^{Celia/Celia}$ (S.A. $Bscl2^{Celia/Celia}$, 6.2 months) and 6 severely affected $Bscl2^{+/Celia}$ mice (S.A. $Bscl2^{+/Celia}$, 6.6 months). Data is presented as mean ± SD. Statistics: non-parametric Kruskal-Wallis test, followed by a post-hoc Mann-Whitney U. * $p < 0.05$ vs wild type; $^{\#}$ $p < 0.05$ vs $Bscl2^{+/Celia}$; $^{\$}$ $p < 0.05$ vs $Bscl2^{Celia/Celia}$; $^{\alpha}$ $p < 0.05$ vs S.A. $Bscl2^{+/Celia}$; $^{\&}$ $p < 0.05$ vs S.A $Bscl2^{Celia/Celia}$. (f) Western blot analysis of 6× His-tagged Celia seipin protein from brain tissues of $Bscl2^{+/Celia}$ ♂ (n = 1, 6.1 months); $Bscl2^{Celia/Celia}$ ♂ (n = 1, 6.1 months) and the hypothalamus of a human without the disease as a negative control. Data is presented in two different gels, one for $Bscl2^{+/Celia}$ and one for $Bscl2^{Celia/Celia}$, with six brain areas and the negative control each.

presence of wild type human seipin kidnapped the aberrant Celia-seipin, avoiding the formation of large protein macroaggregates into the nucleus, thereby explaining the lack of neurological symptoms in human heterozygous carriers. This fact could be related to the appearance of neurological symptoms in some heterozygous mice, since these presented a lower expression of wild type seipin compared to those heterozygous mice that are not severely affected. However, at the present time, there is no evidence that this is also happening in mouse brains, the seipin of which is different from humans, mainly in cytoplasmic amino- and carboxi-terminal ends (Sanchez-Iglesias et al., 2019a). Furthermore, murine *Bscl2* gene expression is lower in brain than in adipose tissue, which is not the case in humans (Chen et al.,

2009). Along the same lines, there are inter-species differences regarding *Bscl2/BSCL2* genes expression in different brain regions. Thus, the mouse *Bscl2* gene is mainly expressed in the basal forebrain, hippocampus, hypothalamus, and dorsal and ventral brainstem, with lower expression in the cortex and striatum (Garfield et al., 2012; Liu et al., 2016). In contrast, in humans, higher *BSCL2* gene expression was found in the caudate and putamen nuclei, cerebellum, and pons, and mainly in the forebrain and rhombencephalon (Sanchez-Iglesias et al., 2019a). This is an important issue due to the fact that a recurrent finding in human PELD is damage to the caudate nucleus (Sánchez-Iglesias et al., 2021). Taking all of these interspecies differences into account, and if it is speculated that the protective mechanism previously mentioned is not present in the mouse brain, it would not be a surprise to find severely affected heterozygous KI mice, but the opposite, with just the expected ratio (5.4 vs 11.9%). This does not preclude that more in-depth experiments should be performed in order to verify this hypothesis.

Another important issue is to know the amount of human Celia-seipin in the different brain areas of these mice. It can be assumed that the promoter is working properly, although this does not necessarily have to be correct, and differences in Celia *BSCL2*-TG expression could be modulated by unknown epigenetic or non-epigenetic mechanisms (Ramakrishna et al., 2021; Srinivasan et al., 2022), which could modify the post-transcriptional regulation of protein expression. The lack of a specific Celia-seipin antibody hinders more detailed studies to reveal the pathogenic mechanism of these findings. Although it has been demonstrated using anti-6His-tagged seipin antibody that human transgene is translated, these experiments were not carried out on affected animals and the amount of aberrant Celia seipin is probably determinant in explaining the severity of neurological symptoms. Although additional experiments are being designed in order to resolve this conundrum, the fact that ubiquitin-reactive nuclear inclusions have been observed in the cerebellums of affected mice, resembling findings reported in PELD patients (Guillen-Navarro et al., 2013; Ruiz-Riquelme et al., 2015a) is highly suggestive of a similar pathogenic mechanism.

Some studies have suggested the association of seipin with various ER-organelles, such as mitochondria and peroxisomes. In seipin KO flies, as well as in mouse and human cell studies, seipin was shown to influence lipid droplet storage via the mitochondrial calcium flux system (Ding et al., 2018; Combot et al., 2022; Salo, 2023). In addition, studies in yeast have shown that cooperation between seipin and Pex30 is necessary for the formation of lipid droplets (Wang et al., 2018a; Joshi et al., 2018). In this regard, some years ago, our group proposed that seipin plays an important role in peroxisome biogenesis in humans (Sanchez-Iglesias et al., 2019a). In particular, some genes encoding protective enzymes against oxidative stress (including *SOD1* and *SOD2*) were related with *BSCL2* expression in human brains. On the other hand, confocal microscopy studies have shown that both seipin and *PEX16,* a key protein for peroxisomal biogenesis (Hua et al., 2015), are closely expressed in the hypothalamus of healthy human brains, while *PEX16* was absent in the same region of a human PELD case (Sanchez-Iglesias et al., 2019a). In view of these results, the present study examined the expression of several genes related with mitochondrial and peroxisome function in different brain areas of affected and non-affected mice. Although the results were not identical to those found in human brains, including one case with PELD, the expression of *Sod2* (and possibly *Sod1*) was significantly reduced in the cortex of both homozygous and heterozygous affected animals, coinciding, at least in homozygous mice, with the highest expression of Celia *BSCL2*-TG. These findings support the hypothesis that aberrant seipin expression in the brain ultimately impairs proteins that protecting against neurodegeneration by reducing the production of reactive oxygen species (Butterfield et al., 2012).

Non-S.A. KI homozygous mice exhibited impaired behavior in some tests (decrease in locomotor activities, less coordination and greater anxiety), but not in those evaluating parameters related to cognitive functions and memory. These findings could be attributed to the lack of wild type murine seipin. Some authors have reported similar findings regarding impaired motor coordination in a neuronal seipin knockout mice (Wang et al., 2018b), along with spatial cognitive deficits, while others (Zhou et al., 2016; Qian et al., 2016; Zhou et al., 2014) have reported deficits in learning and memory as well as anxiety- and depression-like behaviors in seipin knock-out mice. Both behavior and motor deficits were triggered by a reduction in PPARγ activity (Zhou et al., 2016; Qian et al., 2016; Chang et al., 2019). In our animals, however, not all of these behavioral defects were observed. In addition, *Pparg* gene expression was not different among genotypes in the studied brain areas, although no protein levels were analyzed.

Bscl2$^{Celia/Celia}$ mice showed a severe lack of adipose tissue (particularly gonadal WAT), massive hepatic steatosis, hyperinsulinemia, severe hypoleptinemia, hypertransaminasemia and insulin resistance, as well as enlargement of other visceral organs (kidneys, heart and spleen). All of these characteristics resemble those found in both congenital generalized lipodystrophy type 2 and PELD in humans (Patni and Garg, 2022), albeit without diabetes mellitus or hypertriglyceridemia. Although some PELD patients carrying the c.985C > T variant have not lipodystrophy, being the responsible mechanism unclear at present, this does not happen in our murine model in homozygosity, being all of the mice severely lipoatrophic, thus it must consider that Celia-seipin leads to a loss-of-function, at least in extra-neural tissues.

These findings have previously been reported in other models of seipin knock-out (SKO) mice (Cui et al., 2011; Prieur et al., 2013; Chen et al., 2012). As far as fasting triglycerides levels are concerned, it was found that they were significantly reduced (50%) in young animals (4 months), as has been reported by other authors (Cui et al., 2011; Prieur et al., 2013; Chen et al., 2012). However, as the animals became older (9.5 months) triglyceride levels showed a tendency to be higher (53%) than their wild type littermates, albeit without statistical significance. Basal glucose was similar among genotypes and remained so throughout the animals' lives. Other authors have reported glucose intolerance in SKO mouse (Cui et al., 2011; Prieur et al., 2013). However, in the present study, as in other tissue-specific SKO mice (McIlroy et al., 2018), no impaired glucose tolerance was found, although there was insulin resistance. One surprising finding was that S.A. *Bscl2*$^{Celia/Celia}$ mice did not present hyperinsulinemia and their livers had only mild steatosis with a quite normal hepatic weight, despite being severely lipoatrophic. It has been proposed (Magre and Prieur, 2022) that mice have no obvious cell-autonomous function for seipin in the hepatocyte and that the lack of adipose tissue is the major trigger of the metabolic and hepatic complications associated with SKO mice. Our S.A. KI mice presented a dramatic lack of fat and a severe hypoleptinemia, but, at the same time, they were significantly lighter than non-affected *Bscl2*$^{Celia/Celia}$ mice. Although their food uptake was not quantified, given their severe neurological condition, the most parsimonious explanation would be that this was severely reduced. This would explain their lower liver weight, as well as the improvement in hepatic steatosis and insulin resistance. In this regard, Chen et al. (Chen et al., 2014) demonstrated that prolonged fasting in SKO mice improved insulin sensitivity and hepatic steatosis. In patients with congenital generalized lipodystrophy, treatment with recombinant human leptin dramatically reduced appetite, improved glucose tolerance, reduced both triglycerides and insulin levels, increased insulin sensitivity and improved hepatic steatosis, reducing liver volume (Brown et al., 2018).

The authors of the present study are aware of the limitations of this model, not only regarding the number of S.A. mice but also, and probably more importantly, the differences in the pathogenic mechanisms which explain the neurological findings. In this sense, it is necessary to unveil the mechanisms which lie behind the amount of translated seipin, and its lack of correlation with the human transgene expression, particularly in heterozygous KI mice, beyond the fact that getting a perfect animal model of a human disease is always challenging.

In summary, a global murine model of Celia's encephalopathy has been generated for the first time, which partially recapitulates the severe neurodegenerative picture suffered by these patients. Furthermore, it

also provides a good model of congenital generalized lipodystrophy.

Supplementary data to this article can be found online at https://doi.org/10.1016/j.nbd.2023.106300.

Funding

This research was funded by the Instituto de Salud Carlos III, ISCIII (grant numbers PI18/01890 and PI22/00514) and the Fundación Mutua Madrileña (call 2015), and was co-funded by the European Union, and an intramural grant from the Xunta de Galicia (grant numbers ED341b 2017/19 and ED431B 2020/37). A.F.-P. was a Rio Hortega researcher (ISCIII; CM20/00155) at the time this study was carried out and is currently receiving funding from the Fundación Alfonso Martín Escudero. S.S.-I. was awarded a Research Fellowship by the Asociación Española de Familiares y Afectados de Lipodistrofias (AELIP).

Authors' contributions

Conceptualization, S.C.-G., S.S.-I. and D.A.-V.; Data curation: D.A-V; Formal analysis: D.A-V, S.S-I, S.C-G; Funding acquisition: D.A-V; Investigation: D.A-V, S.S-I, S.C-G, P.A., N.G.-L., L.G.-V., A.R, B.·S-M, I.B.-G. and A.S.; Methodology: S.S-I, S.C-G, P.A., N.G.-L. L.G.-V., A.R, B.·S-M, I.B.-G., A.S. and L.L-F; Resources: D.A.-V., A.R, B.·S-M, P.A.; Software: S.S.-I, P.A.; Supervision: S.S.-I. and D.A.-V.; Visualization: S.C.-G., S.S.-I., D.A.-V., A.R., P.A.; Writing-original draft: S.C.-G., S.S.-I., P.A, A.R, and D.A.-V.; Writing-review and editing: S.C.-G., S.S.-I. and D.A.-V.

Ethics approval

All animal work and procedures were approved by the institutional Ethics Committee of the Xunta de Galicia (15010/17/004 and 15012/2021/014) and the University of Santiago and performed following the principles of laboratory animal care mandated by European Union Law (2010/63/UE) and the Spanish Government (RD 53/2013) on the protection of animals used for scientific purposes.

Consent to participate and to publish

Not applicable.

Declaration of Competing Interest

The authors declare that they have no competing interests.

Data availability

The datasets supporting the conclusions of this article are included within the article and its supplementary information.

Acknowledgements

We are indebted to José Ángel Hernández-Malagón for technical assistance.

References

Aartsma-Rus, A., van Putten, M., 2014. Assessing functional performance in the mdx mouse model. J. Vis. Exp. 85 https://doi.org/10.3791/51303.

Alaei, M.R., Talebi, S., Ghofrani, M., Taghizadeh, M., Keramatipour, M., 2016. Whole exome sequencing reveals a BSCL2 mutation causing progressive encephalopathy with lipodystrophy (PELD) in an Iranian pediatric patient. Iran. Biomed. J. 20 (5), 295–301.

Araujo-Vilar, D., Santini, F., 2019. Diagnosis and treatment of lipodystrophy: a step-by-step approach. J. Endocrinol. Investig. 42 (1), 61–73. https://doi.org/10.1007/s40618-018-0887-z.

Araujo-Vilar, D., Domingo-Jimenez, R., Ruibal, A., Aguiar, P., Ibanez-Mico, S., Garrido-Pumar, M., et al., 2018. Association of metreleptin treatment and dietary intervention with neurological outcomes in Celia's encephalopathy. Eur. J. Hum. Genet. 26 (3), 396–406. https://doi.org/10.1038/s41431–017–0052-8.

Benede-Ubieto, R., Estevez-Vazquez, O., Ramadori, P., Cubero, F.J., Nevzorova, Y.A., 2020. Guidelines and considerations for metabolic tolerance tests in mice. Diabetes Metab. Syndr. Obes. 13, 439–450. https://doi.org/10.2147/DMSO.S234665.

Bromley-Brits, K., Deng, Y., Song, W., 2011. Morris water maze test for learning and memory deficits in Alzheimer's disease model mice. J. Vis. Exp. 53 https://doi.org/10.3791/2920.

Brooks, S.P., Dunnett, S.B., 2009. Tests to assess motor phenotype in mice: a user's guide. Nat. Rev. Neurosci. 10 (7), 519–529. https://doi.org/10.1038/nrn2652.

Brown, R.J., Oral, E.A., Cochran, E., Araujo-Vilar, D., Savage, D.B., Long, A., et al., 2018. Long-term effectiveness and safety of metreleptin in the treatment of patients with generalized lipodystrophy. Nucleus. 60 (3), 479–489. https://doi.org/10.1007/s12020-018-1589-1.

Butterfield, D.A., Perluigi, M., Reed, T., Muharib, T., Hughes, C.P., Robinson, R.A., et al., 2012. Redox proteomics in selected neurodegenerative disorders: from its infancy to future applications. Antioxid. Redox Signal. 17 (11), 1610–1655. https://doi.org/10.1089/ars.2011.4109.

Cartwright, B.R., Goodman, J.M., 2012. Seipin: from human disease to molecular mechanism. J. Lipid Res. 53 (6), 1042–1055. https://doi.org/10.1194/jlr.R023754.

Chang, H., Di, T., Wang, Y., Zeng, X., Li, G., Wan, Q., et al., 2019. Seipin deletion in mice enhances phosphorylation and aggregation of tau protein through reduced neuronal PPARgamma and insulin resistance. Neurobiol. Dis. 127, 350–361. https://doi.org/10.1016/j.nbd.2019.03.023.

Chen, W., Yechoor, V.K., Chang, B.H., Li, M.V., March, K.L., Chan, L., 2009. The human lipodystrophy gene product Berardinelli-Seip congenital lipodystrophy 2/seipin plays a key role in adipocyte differentiation. Endocrinology. 150 (10), 4552–4561. https://doi.org/10.1210/en.2009–0236.

Chen, W., Chang, B., Saha, P., Hartig, S.M., Li, L., Reddy, V.T., et al., 2012. Berardinelli-seip congenital lipodystrophy 2/seipin is a cell-autonomous regulator of lipolysis essential for adipocyte differentiation. Mol. Cell. Biol. 32 (6), 1099–1111. https://doi.org/10.1128/MCB.06465–11.

Chen, W., Zhou, H., Saha, P., Li, L., Chan, L., 2014. Molecular mechanisms underlying fasting modulated liver insulin sensitivity and metabolism in male lipodystrophic Bscl2/Seipin-deficient mice. Endocrinology. 155 (11), 4215–4225. https://doi.org/10.1210/en.2014–1292.

Combot, Y., Salo, V.T., Chadeuf, G., Holtta, M., Ven, K., Pulli, I., et al., 2022. Seipin localizes at endoplasmic-reticulum-mitochondria contact sites to control mitochondrial calcium import and metabolism in adipocytes. Cell Rep. 38 (2), 110213 https://doi.org/10.1016/j.celrep.2021.110213.

Cui, X., Wang, Y., Tang, Y., Liu, Y., Zhao, L., Deng, J., et al., 2011. Seipin ablation in mice results in severe generalized lipodystrophy. Hum. Mol. Genet. 20 (15), 3022–3030. https://doi.org/10.1093/hmg/ddr205.

Curzon, P., Zhang, M., Radek, R.J., Fox, G.B., 2009. The behavioral assessment of sensorimotor processes in the mouse: Acoustic startle, sensory gating, locomotor activity, rotarod, and beam walking. In: Buccafusco, J.J. (Ed.), Methods of Behavior Analysis in Neuroscience. Frontiers in Neuroscience, 2nd ed. Boca Raton (FL).

Deacon, R.M., 2013a. Measuring motor coordination in mice. J. Vis. Exp. 75 https://doi.org/10.3791/2609 e2609.

Deacon, R.M., 2013b. Shallow water (paddling) variants of water maze tests in mice. J. Vis. Exp. 76.

Ding, L., Yang, X., Tian, H., Liang, J., Zhang, F., Wang, G., et al., 2018. Seipin regulates lipid homeostasis by ensuring calcium-dependent mitochondrial metabolism. EMBO J. 37 (17) https://doi.org/10.15252/embj.201797572.

Encarnacion, A., Horie, N., Keren-Gill, H., Bliss, T.M., Steinberg, G.K., Shamloo, M., 2011. Long-term behavioral assessment of function in an experimental model for ischemic stroke. J. Neurosci. Methods 196 (2), 247–257. https://doi.org/10.1016/j.jneumeth.2011.01.010.

Febinger, H.Y., Thomasy, H.E., Gemma, C., 2016. A controlled cortical impact mouse model for mild traumatic brain injury. Bio-protocol 6 (16). https://doi.org/10.21769/BioProtoc.1901 e1901.

Fernandez-Marmiesse, A., Sanchez-Iglesias, S., Darling, A., O'Callaghan, M.M., Tonda, R., Jou, C., et al., 2019. A de novo heterozygous missense BSCL2 variant in 2 siblings with intractable developmental and epileptic encephalopathy. Seizure. 71, 161–165. https://doi.org/10.1016/j.seizure.2019.07.019.

Garfield, A.S., Chan, W.S., Dennis, R.J., Ito, D., Heisler, L.K., Rochford, J.J., 2012. Neuroanatomical characterisation of the expression of the lipodystrophy and motor-neuropathy gene Bscl2 in adult mouse brain. PLoS One 7 (9), e45790. https://doi.org/10.1371/journal.pone.0045790.

Gaskill, B.N., Karas, A.Z., Garner, J.P., Pritchett-Corning, K.R., 2013. Nest building as an indicator of health and welfare in laboratory mice. J. Vis. Exp. 82, 51012. https://doi.org/10.3791/51012.

Golde, W.T., Gollobin, P., Rodriguez, L.L., 2005. A rapid, simple, and humane method for submandibular bleeding of mice using a lancet. Lab. Anim. (NY) 34 (9), 39–43. https://doi.org/10.1038/laban1005–39.

Greenfield, E.A., 2017. Sampling and preparation of mouse and rat serum. Cold Spring Harb Protoc 2017 (11). https://doi.org/10.1101/pdb.prot100271 pdb prot100271.

Guillen-Navarro, E., Sanchez-Iglesias, S., Domingo-Jimenez, R., Victoria, B., Ruiz-Riquelme, A., Rabano, A., et al., 2013. A new seipin-associated neurodegenerative syndrome. J. Med. Genet. 50 (6), 401–409. https://doi.org/10.1136/jmedgenet-2013-101525.

Hua, R., Gidda, S.K., Aranovich, A., Mullen, R.T., Kim, P.K., 2015. Multiple domains in PEX16 mediate its trafficking and recruitment of peroxisomal proteins to the ER. Traffic. 16 (8), 832–852. https://doi.org/10.1111/tra.12292.

Huang, H.H., Chen, T.H., Hsiao, H.P., Huang, C.T., Wang, C.C., Shiau, Y.H., et al., 2010. A Taiwanese boy with congenital generalized lipodystrophy caused by homozygous

Ile262fs mutation in the BSCL2 gene. Kaohsiung J. Med. Sci. 26 (11), 615–620. https://doi.org/10.1016/S1607-551X(10)70094–2.
Joshi, A.S., Nebenfuehr, B., Choudhary, V., Satpute-Krishnan, P., Levine, T.P., Golden, A., et al., 2018. Lipid droplet and peroxisome biogenesis occur at the same ER subdomains. Nat. Commun. 9 (1), 2940. https://doi.org/10.1038/s41467–018–05277-3.
Kleiner, D.E., Brunt, E.M., Van Natta, M., Behling, C., Contos, M.J., Cummings, O.W., et al., 2005. Design and validation of a histological scoring system for nonalcoholic fatty liver disease. Hepatology. 41 (6), 1313–1321. https://doi.org/10.1002/hep.20701.
L, S.C., 2014. A Practical Guide to the Histology of the Mouse. Wiley Blackwell, Chichester, West Sussex, UK.
Liu, X., Xie, B., Qi, Y., Du, X., Wang, S., Zhang, Y., et al., 2016. The expression of SEIPIN in the mouse central nervous system. Brain Struct. Funct. 221 (8), 4111–4127. https://doi.org/10.1007/s00429–015–1151-3.
Livak, K.J., Schmittgen, T.D., 2001. Analysis of relative gene expression data using real-time quantitative PCR and the 2(-Delta Delta C(T)) Method. Methods. 25 (4), 402–408. https://doi.org/10.1006/meth.2001.1262.
Ma, Y., Hof, P.R., Grant, S.C., Blackband, S.J., Bennett, R., Slatest, L., et al., 2005. A three-dimensional digital atlas database of the adult C57BL/6J mouse brain by magnetic resonance microscopy. Neuroscience. 135 (4), 1203–1215. https://doi.org/10.1016/j.neuroscience.2005.07.014.
Magre, J., Prieur, X., 2022. Seipin deficiency as a model of severe adipocyte dysfunction: lessons from rodent models and teaching for human disease. Int. J. Mol. Sci. 23 (2) https://doi.org/10.3390/ijms23020740.
Magre, J., Delepine, M., Khallouf, E., Gedde-Dahl Jr., T., Van Maldergem, L., Sobel, E., et al., 2001. Identification of the gene altered in Berardinelli-Seip congenital lipodystrophy on chromosome 11q13. Nat. Genet. 28 (4), 365–370. https://doi.org/10.1038/ng585.
McIlroy, G.D., Suchacki, K., Roelofs, A.J., Yang, W., Fu, Y., Bai, B., et al., 2018. Adipose specific disruption of seipin causes early-onset generalised lipodystrophy and altered fuel utilisation without severe metabolic disease. Mol. Metab. 10, 55–65. https://doi.org/10.1016/j.molmet.2018.01.019.
Mirrione, M.M., Schiffer, W.K., Fowler, J.S., Alexoff, D.L., Dewey, S.L., Tsirka, S.E., 2007. A novel approach for imaging brain-behavior relationships in mice reveals unexpected metabolic patterns during seizures in the absence of tissue plasminogen activator. Neuroimage. 38 (1), 34–42. https://doi.org/10.1016/j.neuroimage.2007.06.032.
Nunez, J., 2008. Morris water maze experiment. J. Vis. Exp. 19.
O'Leary, T.P., Gunn, R.K., Brown, R.E., 2013. What are we measuring when we test strain differences in anxiety in mice? Behav. Genet. 43 (1), 34–50. https://doi.org/10.1007/s10519–012–9572-8.
Parasuraman, S., Raveendran, R., Kesavan, R., 2010. Blood sample collection in small laboratory animals. J. Pharmacol. Pharmacother. 1 (2), 87–93. https://doi.org/10.4103/0976-500X.72350.
Patni, N., Garg, A., 2022. Lipodystrophy for the diabetologist-what to look for. Curr. Diab. Rep. 22 (9), 461–470. https://doi.org/10.1007/s11892–022-01485-w.
Poisson, A., Chatron, N., Labalme, A., Till, M., Broussolle, E., Sanlaville, D., et al., 2019. Regressive autism spectrum disorder expands the phenotype of BSCL2/seipin-associated neurodegeneration. Biol. Psychiatry 85 (4). https://doi.org/10.1016/j.biopsych.2018.05.010 e17-e9.
Prieur, X., Dollet, L., Takahashi, M., Nemani, M., Pillot, B., Le May, C., et al., 2013. Thiazolidinediones partially reverse the metabolic disturbances observed in Bscl2/seipin-deficient mice. Diabetologia. 56 (8), 1813–1825. https://doi.org/10.1007/s00125–013–2926-9.
Qian, Y., Yin, J., Hong, J., Li, G., Zhang, B., Liu, G., et al., 2016. Neuronal seipin knockout facilitates Abeta-induced neuroinflammation and neurotoxicity via reduction of PPARgamma in hippocampus of mouse. J. Neuroinflammation 13 (1), 145. https://doi.org/10.1186/s12974–016–0598-3.
Ramakrishna, S., Jhaveri, V., Konings, S.C., Nawalpuri, B., Chakraborty, S., Holst, B., et al., 2021. APOE4 affects basal and NMDAR-mediated protein synthesis in neurons by perturbing calcium homeostasis. J. Neurosci. 41 (42), 8686–8709. https://doi.org/10.1523/JNEUROSCI.0435–21.2021.
Rao, M.J., Goodman, J.M., 2021. Seipin: harvesting fat and keeping adipocytes healthy. Trends Cell Biol. 31 (11), 912–923. https://doi.org/10.1016/j.tcb.2021.06.003.
Ruiz-Riquelme, A., Sánchez-Iglesias, S., Rábano, A., Guillén-Navarro, E., Domingo-Jiménez, R., Ramos, A., et al., 2015a. Larger aggregates of mutant seipin in Celia's encephalopathy, a new protein misfolding neurodegenerative disease. Neurobiol. Dis. 83, 44–53. https://doi.org/10.1016/j.nbd.2015.08.006.
Ruiz-Riquelme, A., Sanchez-Iglesias, S., Rabano, A., Guillen-Navarro, E., Domingo-Jimenez, R., Ramos, A., et al., 2015b. Larger aggregates of mutant seipin in Celia's encephalopathy, a new protein misfolding neurodegenerative disease. Neurobiol. Dis. 83, 44–53. https://doi.org/10.1016/j.nbd.2015.08.006.
Salo, V.T., 2023. Seipin-still a mysterious protein? Front Cell. Dev. Biol. 11, 1112954. https://doi.org/10.3389/fcell.2023.1112954.
Sanchez-Iglesias, S., Fernandez-Liste, A., Guillin-Amarelle, C., Rabano, A., Rodriguez-Canete, L., Gonzalez-Mendez, B., et al., 2019a. Does seipin play a role in oxidative stress protection and peroxisome biogenesis? New insights from human brain autopsies. Neuroscience. 396, 119–137. https://doi.org/10.1016/j.neuroscience.2018.11.004.
Sanchez-Iglesias, S., Crocker, M., O'Callaghan, M., Darling, A., García-Cazorla, A., Domingo-Jiménez, R., et al., 2019b. Celia's encephalopathy and c.974dupG in BSCL2 gene: a hidden change in a known variant. Neurogenetics. https://doi.org/10.1007/s10048–019–00574-5 in press.
Sánchez-Iglesias, S., Fernández-Pombo, A., Cobelo-Gómez, S., Hermida-Ameijeiras, Á., Alarcón-Martínez, H., Domingo-Jiménez, R., et al., 2021. Celia's encephalopathy (BSCL2-gene-related): current understanding, 10 (7), 1435.
Schaar, K.L., Brenneman, M.M., Savitz, S.I., 2010. Functional assessments in the rodent stroke model. Exp. Transl. Stroke Med. 2 (1), 13. https://doi.org/10.1186/2040-7378-2-13.
Seibenhener, M.L., Wooten, M.C., 2015. Use of the open field maze to measure locomotor and anxiety-like behavior in mice. J. Vis. Exp. 96 https://doi.org/10.3791/52434 e52434.
Shepherd, J.K., Grewal, S.S., Fletcher, A., Bill, D.J., Dourish, C.T., 1994. Behavioural and pharmacological characterisation of the elevated "zero-maze" as an animal model of anxiety. Psychopharmacology 116 (1), 56–64. https://doi.org/10.1007/BF02244871.
Sim, M.F., Talukder, M.M., Dennis, R.J., O'Rahilly, S., Edwardson, J.M., Rochford, J.J., 2013. Analysis of naturally occurring mutations in the human lipodystrophy protein seipin reveals multiple potential pathogenic mechanisms. Diabetologia. 56 (11), 2498–2506. https://doi.org/10.1007/s00125–013–3029-3.
Sim, M.F.M., Persiani, E., Talukder, M.M.U., McIlroy, G.D., Roumane, A., Edwardson, J. M., et al., 2020. Oligomers of the lipodystrophy protein seipin may co-ordinate GPAT3 and AGPAT2 enzymes to facilitate adipocyte differentiation. Sci. Rep. 10 (1), 3259. https://doi.org/10.1038/s41598–020–59982-5.
Srinivasan, A.R., Tran, T.T., Bonini, N.M., 2022. Loss of miR-34 in Drosophila dysregulates protein translation and protein turnover in the aging brain. Aging Cell 21 (3), e13559. https://doi.org/10.1111/acel.13559.
Tatem, K.S., Quinn, J.L., Phadke, A., Yu, Q., Gordish-Dressman, H., Nagaraju, K., 2014. Behavioral and locomotor measurements using an open field activity monitoring system for skeletal muscle diseases. J. Vis. Exp. 91, 51785. https://doi.org/10.3791/51785.
Victoria, B., Cabezas-Agricola, J.M., Gonzalez-Mendez, B., Lattanzi, G., Del Coco, R., Loidi, L., et al., 2010. Reduced adipogenic gene expression in fibroblasts from a patient with type 2 congenital generalized lipodystrophy. Diabet. Med. 27 (10), 1178–1187. https://doi.org/10.1111/j.1464–5491.2010.03052.x.
Wang, S., Idrissi, F.Z., Hermansson, M., Grippa, A., Ejsing, C.S., Carvalho, P., 2018a. Seipin and the membrane-shaping protein Pex30 cooperate in organelle budding from the endoplasmic reticulum. Nat. Commun. 9 (1), 2939. https://doi.org/10.1038/s41467–018–05278-2.
Wang, L., Hong, J., Wu, Y., Liu, G., Yu, W., Chen, L., 2018b. Seipin deficiency in mice causes loss of dopaminergic neurons via aggregation and phosphorylation of alpha-synuclein and neuroinflammation. Cell Death Dis. 9 (5), 440. https://doi.org/10.1038/s41419–018–0471-7.
Wu, Y.R., Hung, S.I., Chang, Y.C., Chen, S.T., Lin, Y.L., Chung, W.H., 2009. Complementary mutations in seipin gene in a patient with Berardinelli-Seip congenital lipodystrophy and dystonia: phenotype variability suggests multiple roles of seipin gene. J. Neurol. Neurosurg. Psychiatry 80 (10), 1180–1181. https://doi.org/10.1136/jnnp.2008.165977.
Yan, R., Qian, H., Lukmantara, I., Gao, M., Du, X., Yan, N., et al., 2018. Human SEIPIN binds anionic phospholipids. Dev. Cell 47 (2), 248–256 e4. https://doi.org/10.1016/j.devcel.2018.09.010.
Zhou, L., Yin, J., Wang, C., Liao, J., Liu, G., Chen, L., 2014. Lack of seipin in neurons results in anxiety- and depression-like behaviors via down regulation of PPARgamma. Hum. Mol. Genet. 23 (15), 4094–4102. https://doi.org/10.1093/hmg/ddu126.
Zhou, L., Chen, T., Li, G., Wu, C., Wang, C., Li, L., et al., 2016. Activation of PPARgamma ameliorates spatial cognitive deficits through restoring expression of AMPA receptors in seipin knock-out mice. J. Neurosci. 36 (4), 1242–1253. https://doi.org/10.1523/JNEUROSCI.3280–15.2016.